DOE/BC/14994-13
OSTI ID: 9325

SPONTANEOUS IMBIBITION IN LOW PERMEABILITY MEDIA

SUPRI TR 114

By
Josephia Schembre
Anthony R. Kovscek

December 1998

Work Performed Under Contract No. DE-FG22-96BC14994

Stanford University
Stanford, California

National Petroleum Technology Office
U. S. DEPARTMENT OF ENERGY
Tulsa, Oklahoma

DISCLAIMER

Portions of this document may be illegible in electronic image products. Images are produced from the best available original document.

DOE/BC/14994-13
Distribution Category UC-122

Spontaneous Imbibition in Low Permeability Media

SUPRI TR 114

By
Josephia Schembre
Anthony R. Kovscek

December 1998

Work Performed Under Contract DE-FG22-96BC14994

Prepared for
U.S. Department of Energy
Assistant Secretary for Fossil Energy

Thomas Reid, Project Manager
National Petroleum Technology Office
P.O. Box 3628
Tulsa, OK 74101

Prepared by
Stanford University
Petroleum Engineering Department
65 Green Earth Sciences Bldg.
Stanford, CA 94305

TABLE OF CONTENTS

LIST OF FIGURES

LIST OF TABLES

ACKNOWLEDGMENTS

This work was supported by the Fossil Energy, Office of Oil, Gas and Shale Technologies of the U.S. Department of Energy, under contract No. DE-FG22-96BC14994 to Stanford University. The support of the SUPRI-A Industrial Affiliates is likewise gratefully acknowledged.

ABSTRACT

A systematic experimental investigation of capillary pressure characteristics and fluid flow in diatomite was begun. Using an X-ray CT scanner and a specially constructed imbibition cell, we study spontaneous water imbibition processes in diatomite and, for reference, Berea sandstone and chalk. The mass of water imbibed as a function of time is also measured. Imbibition is restricted to cocurrent flow. Despite a marked difference in rock properties such as permeability and porosity, we find similar trends in saturation profiles and weight gain versus time functions. Imbibition in diatomite is relatively rapid when initial water saturation is low due to large capillary forces.

Using a non-linear regression analysis together with the experimental data, the capillary pressure and water relative permeability curves are determined for the diatomite in the water-air system. The results given for displacement profiles by numerical simulation match the experimental results.

1 INTRODUCTION

1.1 Introduction

The increasing depletion of oil reservoirs requires the constant development of additional crude reserves and implementation of efficient oil recovery techniques to meet the growing global demand for energy. Fractured petroleum reservoirs contain a substantial fraction (over 20%) of the world's oil reserves (Saidi, 1983). Nonetheless, the efficiency of recovery processes in such reservoirs remains difficult to evaluate because of the lack of general understanding of multiphase flow through fractured porous media. The existence of fractured low permeability siliceous shale reservoirs imposes a need for better understanding of the factors influencing hydrocarbon recovery from such rocks. An important class of siliceous shale that remains relatively unstudied is diatomite

Diatomite is a hydrous, non-crystalline form of silica or opal composed of the remains of microscopic shells of diatoms, which are single-celled aquatic plankton (Stosur and David, 1971). Reservoir rock is assumed to be strongly to moderately water wet. Diatomites have a very high porosity (it frequently exceeds 50 percent) with high internal surface area, but are exceptionally impermeable (Schwartz, 1988) (permeabilities generally range from 0.1 to 10 mD). This low permeability makes efficient oil production very difficult by conventional means. Diatomite is commercially important (Shell Expanding Belridge Diatomite Program, 1994): estimates of the original oil in place (OOIP) for the California Diatomites (Kern Co., CA) range from 10 to 15 billion barrels

(Ilderton *et al.*, 1996). Because the formations are very porous and the initial oil saturation is large (35 to 70%), the target for potential production is high.

Water imbibition is fundamental to both waterflood and steamdrive performance in low permeability reservoir rocks such as diatomite and chalk. Imbibition is an immiscible displacement process, whereby a non-wetting fluid within a porous medium is spontaneously expelled by wetting fluid that surrounds the medium. Wetting fluid is drawn into the medium by capillary suction. This phenomenon is caused by the differential attraction forces between the pore walls and fluids. The rate of imbibition is primarily dependent on the rock permeability, pore structure, wettability, and the interfacial tension between the resident phase and the imbibing phase. On the macroscopic scale, capillary imbibition forces determine, in part, how rapidly and easily a hydraulically fractured water injector injects water into a low permeability formation and at what rate the injected water propagates. In naturally fractured systems with a high degree of interconnectedness, imbibition forces must be strong for a waterflood to be successful. If they are not, water will propagate through the fracture network from injector to producer, and the waterflood will fail.

Capillary phenomena are equally important during steam injection into diatomite or low permeability sandstones. Multiphase flow in diatomite is dominated by capillary forces. Steam injection, especially at short times, is accompanied by condensation and flow of the resulting hot water away from the injector. Likewise, for live steam to enter the matrix of a low permeability rock, a substantial capillary entry pressure must be overcome. Producers might also suffer from capillary effects as the formation attempts to

maintain capillary equilibrium with fluids in the production hydraulic fracture and the well.

Because of the importance of imbibition on oil recovery, it has been studied widely. To date, much of the focus on imbibition has centered on carbonaceous rocks; however, our knowledge of hydrocarbon recovery and fluid displacement is less than complete.

There have been many studies where imbibition has been tested for consolidated sands, and studies of such a mechanism in low-permeability rocks have focused mainly on chalks. A detailed scan of the literature shows few reported capillary pressure curves and little information on the extent and rate of imbibition in diatomite. Likewise, the mechanisms of oil displacement and trapping are unclear, but presumed to be similar to those in sandstone. However, rock morphology is very different (Bhat *et al.* ,1997).

Thus, it seems helpful to undertake a systematic study of fluid transport in diatomite; it appears that capillary driven flow is relevant to reservoir flow processes. In this work, our main focus is the study of one-dimensional spontaneous imbibition of water into air-filled diatomite. This simpler system provides some understanding of the behavior of water-oil-rock systems (Handy, 1960).

The project was divided in three stages. In the first stage, I conducted experiments with a typical sandstone which, together with previous studies reported in the literature allowed us to calibrate and improve our equipment, and simultaneously, acquire detailed knowledge about the mechanism of imbibition. The theoretical understanding and experimental practice obtained in the first stage was useful in the second stage, where the

same properties and mechanisms are studied for a diatomite outcrop sample. Studies performed in chalk are included in this work as well. By comparing these results, I illustrate the effects of pore structure, permeability, and porosity on imbibition.

This study also includes preliminary work on water imbibition into core samples containing oil. The progress and effectiveness of imbibition fronts is monitored using an X-ray CT scanner and a specially constructed imbibition cell. The description of the experimental apparatus, procedure and results obtained for the three rock samples are discussed in Chapter 2 of this report.

The third stage of this project was the simulation of the experiments using a commercial simulator (ECLIPSE). By matching both the displacement observed in the CT images and the weight gained at a particular time, the relative permeability and capillary pressure curves are determined. In this stage, the influence of each of the parameters involved such as pore structure, permeability, relative permeability, and wettability was studied. The model used in the simulator and the results obtained in different simulations are discussed in detail in Chapter 3.

To complete the introduction, a brief review of imbibition and the fundamentals of CT scanning is presented.

1.2 Literature Survey

1.2.1 Imbibition

As previously defined, spontaneous imbibition is that process by which one fluid displaces another from a porous medium as a result of capillary forces only. An equation

that describes the movement of water into dry soils has been derived (Kirkham and Feng, 1949; Cruz and Perez, 1992) and the authors noted the similarity of the equation obtained to the diffusion equation. In this model, it is assumed that the diffusion coefficient is proportional to the partial derivative of capillary pressure with respect to water saturation and computed displacement fronts are significantly diffuse. From this analogy, it is predicted that the volume of water imbibed yields a straight line versus the square root of time. This prediction is confirmed by experimental results for sandstones (Handy, 1960; Garg *et al.*, 1996).

However, the diffusion-type equation may be questionable for some cases. An alternative equation assuming piston-like displacement can be derived which leads to the same dependence of volume imbibed on the square root of time. Handy (1960) provides this classic analysis as well as an experimental investigation of the dynamics of imbibition in sandstone. He examines imbibition in the limit that capillary forces dominate over buoyancy and viscous forces. Displacement occurs vertically upward. In this analysis, the velocity of the imbibed phase is proportional to the gradient of capillary pressure with respect to distance, and fronts are assumed to be sharp.

It is noted that imbibition could be described by either a diffusion-like equation or a frontal-advance equation, depending on assumptions. The main difference between the two descriptions is that the diffusion equation predicts that the smallest pores fill first and the larger pores fill later. The frontal advance equation assumes that pores of all sizes fill simultaneously because large pores are connected to small pores, and *vice versa*. Thus, it is hard to fill the small pores selectively.

Both developments predict that the mass of water imbibed is a linear function of the square root of time and experiments agree with this dependence. However, the end of imbibition is quite abrupt which is contrary to the expected result for a diffusive-type process. This observation lead Handy to assert that the frontal advance equation more nearly described the true process. Indeed, recent experiments where the position and shape of a water imbibition front in a homogeneous Berea sandstone were accurately tracked indicate relatively sharp and steep fronts (Garg *et al.*, 1996). These experiments were also modeled numerically with a diffusion equation incorporating buoyancy driven advection. The authors note that the computed saturation profiles are not sufficiently sharp at the displacement front to match the experimentally determined profiles. Also, water breakthrough occurs too early in the calculations.

Hence, we follow Handy and recognize that the rate of imbibition in porous media, especially air-water systems, is in many respects similar to capillary rise in small diameter tubes. If imbibition occurs vertically upward, the flow equation is

$$u_w = \frac{k_w}{\mu_w}\left(\frac{p_c}{x} - \Delta\rho g\right) \tag{1.1}$$

where p_c is the capillary pressure, u_w is the flow rate, k_w is effective water permeability, μ_w is water viscosity, $\Delta\rho$ is density difference for water and air, g is acceleration due to gravity, and x is position of front. In Eq (1.1), the capillary pressure, p_c is assumed to be constant. Assuming piston-like displacement,

$$u_w = \phi S_w \frac{\partial x}{\partial t} \tag{1.2}$$

where ϕ is the porosity, S_w is the fractional water content of the pore space, x is the distance, and t represents the time. Substituting Eq (1.2) in Eq (1.1) results in,

$$\frac{\partial x}{\partial t} = \frac{k_w}{\phi \mu_w S_w}\left(\frac{p_c}{x} - \Delta\rho g\right) \tag{1.3}$$

Integrating Eq (1.3), one obtains

$$x + \frac{p_c}{\Delta\rho g}\ln\left(1 - \frac{\Delta\rho g x}{P_c}\right) = -\frac{k_w \Delta\rho g}{\phi S_w \mu_w} t \tag{1.4}$$

For $\frac{\Delta\rho g x}{p_c} << 1$, gravity forces are much less than capillary forces and Eq (1.4) reduces to

$$x^2 = \left(\frac{2 p_c k_w}{\phi S_w \mu_w}\right) t \tag{1.5}$$

Since $x^2 = \frac{Q_w}{\phi A_c S_w}$ where Q_w equals total volume of water imbibed,

$$Q_w^2 = \left(\frac{2 p_c k_w \phi A_c^2 S_w}{\mu_w}\right) t \tag{1.6}$$

Here, A is the cross-sectional area of the sample. The rate of imbibition is a function of the product of the effective water permeability, water saturation, and the capillary pressure of the porous medium.

The linear relation between the mass imbibed and the square root of time is apparent and the slope is proportional to the square root of the product of $p_c k_w S_w$. In most situations, the mass, time, and cross-sectional area are easily measured; the density

and viscosity of water are known constants under isothermal conditions; and the porosity is measurable volumetrically. Thus, the only unknown quantities remaining in Eq (1.6) are $p_c k_w S_w$. Dimensional analysis teaches that this quantity has units of force. It is a measure of the likelihood of imbibition. Intuitively, it is expected that the larger is $p_c k_w S_w$, the more rapidly a porous medium imbibes.

We call the product of these unknowns the imbibition potential. The importance of this definition is that it allows us to quantify the rate of imbibition as a function of known values in different rocks.

Thus, we have from Eq (1.6) that the imbibition potential can be expressed as

$$(p_c k_w S_w) = \frac{\lambda^2 \mu_w}{2\phi A_c^{\,2}} \qquad (1.7)$$

where , $\lambda_{imb} = \frac{Q_w}{\sqrt{t}}$ is the slope of the measured weight gain vs. square root of time function.

1.2.2 CT Scanner

During the performance of some of these experiments, it was extremely useful to track simultaneously the movement of the fluids inside the rock sample while the weight gain was recorded. Also, the distribution of porosity is interesting to measure. There are several methods used to visualize or to quantify saturation during laboratory core flood

experiments (Hove *et al*, 1987). In this study, we used X-ray computerized tomography (CT Scanner).

An object of moderate density is placed between an X-ray source and an array of collimated stationary detectors. Power is pulsed to the X-ray tube, creating a thin beam that passes through the object and is received by the detectors. Between each pulse, the X-ray source moves, probing the same portion of the object from a slightly different angle. After the X-ray source completes a 360 excursion of the object (called a pass), mathematical processing of the different X-ray projections is performed by a computer, that produces a synthesized image (slice). The CT image is composed of many volume elements displayed as a 2D image matrix of pixels, and each pixel has its own characteristic attenuation which is related to the density. As a sum of these pixels, the CT image gives the density distribution of the object scanned.

The unit of the relative scale is the CT number. In most CT scanners, the range of CT units is from -1,000 (air), to +3,000 (very dense material) with a value of zero for water.

In this study, the scanning plane is in the longitudinal direction of the core, this gives us a quick visualization of the displacement process from inlet to outlet. There is no need to translate the object. To distinguish between the different materials with the CT method, we need a difference of densities. In order to enhance the visualization of the saturation changes during displacement, we use the method of subtraction of raw images [c.f. (Garg, *et al.*, 1996)] and compute saturations from CT numbers. We have the

following expression for the saturation:

$$S_w = \frac{CT_{obj} - CT_{dry}}{CT_{wet} - CT_{dry}} \tag{1.8}$$

where CT_{wet} is the value for a fully water saturated core, obtained from a last scan performed after 12 hours or more of water imbibition, CT_{dry} is the CT value for the dry core, obtained from the scanning of the core before the imbibition process starts, and CT_{obj} is the CT value of the image being processed.

The map of porosity is obtained by the same method, but in this case, we need a different contrast inside the pores. The calculation involves the CT number of pure water and air,

$$\phi = \frac{CT_{wet} - CT_{dry}}{CT_{water} - CT_{air}} \tag{1.9}$$

where CT_{air} is the CT value of air and CT_{water} is the pure CT value of water. It is important to note that all these calculations assume CT_{wet} corresponds to an image with 100% water saturation.

2 EXPERIMENTAL SECTION

In this chapter, we describe the equipment used, methodology, and results obtained during the experimental stage of this study.

2.1 Preparation of Samples

The rock samples used in this study were Berea sandstone, diatomite, and chalk. Their description is given in Table 2.1. The Berea cores were both cylindrical and square shaped, (core 1 and core 2, respectively). The diatomite (core 3), an outcrop from Lompoc, California, and chalk (core 4), an outcrop from Kansas (core 4) are cylindrical. The objective of using differently shaped, but similar cross-sectional area, Berea sandstone cores were used to confirm that cross-sectional shape did not influence results.

Table 2.1. Rock Sample Characteristics

Core	Rock Type	Shape	Length (cm)	Diameter (cm)	Side (cm)	Porosity (%)
1	Berea	Cylindrical	11.0	2	---	15
2	Berea	Square	9.0	----	1.7	15
3	Diatomite	Cylindrical	8.43	2.5	---	65
4	Chalk	Cylindrical	10.0	2.5	---	21

The Berea sandstone and chalk were cored using conventional drilling and cutting methods. In the case of the diatomite, the core could not be formed by the same method due to its fragile structure. Thus, a piece of the rock was cut by bandsaw to approximate dimensions and it was shaped manually by fixing two circular 1 inch-diameter patterns,

held at both ends of the rock. These pieces were used as guides in the shaping process with a file. Final shaping is achieved with sandpaper.

The sandstone samples were fired at $450^{o}C$ for 12 hours to remove the effect of clay swelling and migration during the imbibition process. Diatomite and chalk were not fired.

The cores were sealed with epoxy on the sides parallel to the flow direction to obtain one-dimensional imbibition (Fig. 2.1). A two-part adhesive epoxy* was used. It is important to mention that, in the case of the diatomite, the coating is a very critical process since the epoxy does not adhere securely to the surface. Without care, delamination of the epoxy coat occurs after some use of the sample. Another method of coating the diatomite core was tried in which we used high-viscosity polymer, but the formation of a skin on the outer side of the core caused the fracture of the core.

2.2 Experimental Method

Our objective is to obtain the change of average water saturation with time, the time rate of imbibition, and to calculate the imbibition potential term from the slope of the average water saturation versus the square root of time. Thus far, we have concentrated on water imbibition into air-filled cores. A limited number of water-oil experiments have also been conducted.

* Epoxy 907 : Adhesive System
Miller Stephenson Chemical Co., Inc.

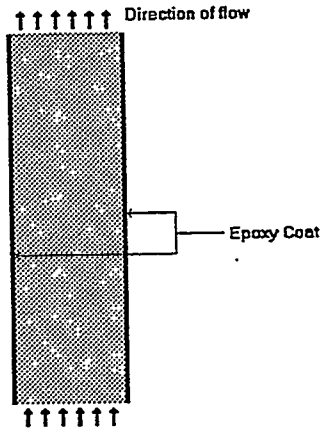

Fig. 2.1 Schematic representation of flow paths

through the core (one-dimensional flow).

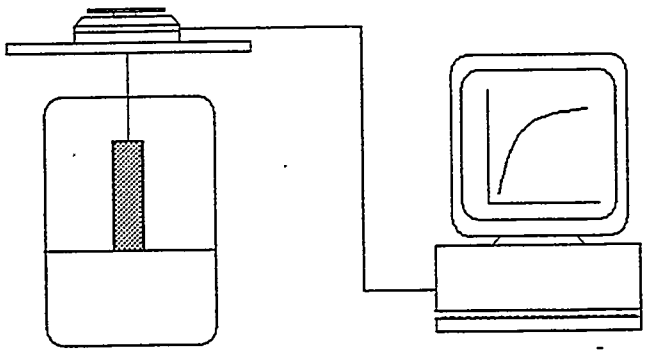

Fig. 2.2 Schematic representation of the experimental design for the first stage.

The weight gain of the core was measured by two methods. Initially, the sample core was suspended by means of an acrylic and steel frame directly from a weighing balance in an acrylic container filled with water (Fig. 2.2). Although this method gives good results, we found some disadvantages in the handling of the core when CT-imaging was performed. Mainly, asymmetry in the scanning plane leads to numerous, uncorrectable, X-shaped, beam hardening artifacts. The design of an imbibition cell which permitted CT-scanning of the core during the imbibition process and minimized artifacts was necessary.

2.2.1 Description of Experimental Cell

The experimental cell, shown schematically in Fig. 2.3, is constructed from acrylic tubes, and it consists of two separate chambers. The main chamber is the core holder and it is surrounded by the second chamber that is filled with water to reduce possible beam hardening. Beam hardening refers to the differential adsorption of longer wavelength X-rays and leads to shadows around the periphery of CT images. There is no fluid exchange between containers, and the outer water-filled chamber allows for some measure of temperature control. The core holder has two end caps for fluids to flow in and out of the core holder. The inlet cap at the bottom of the core holder is connected to a fluid tank through a rubber tube. The weight of imbibed fluid is measured directly by means of a balance as shown in Fig. 2.4. Displaced fluids exit from the top of the core holder.

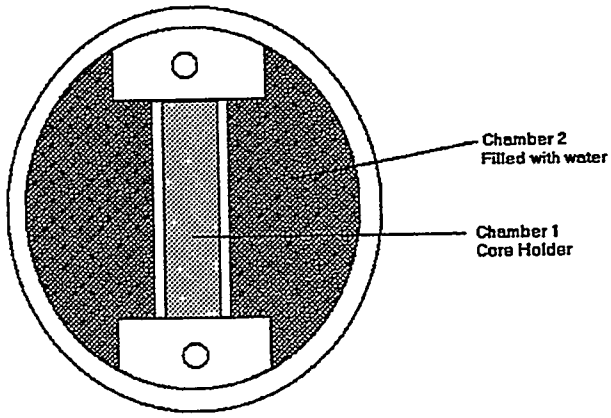

Fig. 2.3: Outline of the imbibition cell showing the two chambers.

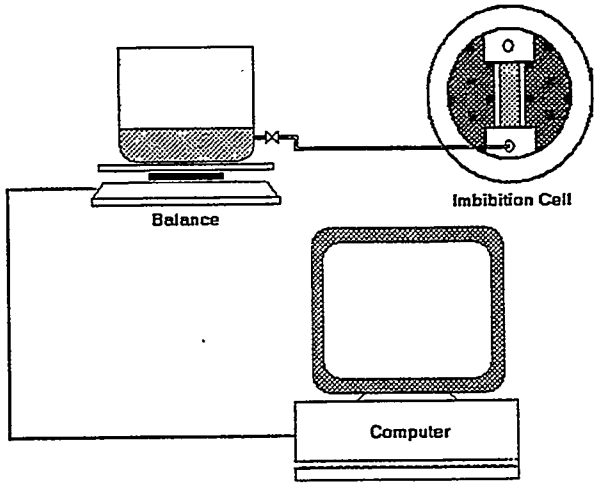

Fig. 2.4: Schematic representation of experimental design for CT-scanning and recording of the change in the weight of the core.

The CT-Scanner used is a Picker™ 1200 SX X-ray scanner with 1200 fixed detectors. The voxel dimension is (0.5 mm by 0.5 mm by 5 mm), the tube current is 65 saturation mA, and the energy level of the radiation is 140 keV. The porosity and aqueous- phase fields are measured on a single vertical volume section in the center of the core as a function of time. The acquisition time of one image is 3 seconds while the processing time is around 40 seconds. The total time of measurement is short enough to capture accurately the position of the front and construct the saturation profiles along the core.

2.2.2 Experimental Procedure.

After preparation and coating, the core is exposed to house vacuum and a temperature of $50^{o}C$, for 10 hours. This ensures a "dry" core at the beginning of the experiment. The procedure is as follows:

a. The dry core is placed in the core holder (main chamber).

b. Filter paper is placed at the bottom of the core. The objective is to obtain a uniform distribution of water at the bottom rock face.

c. Since the core holder is surrounded by water during the CT-experiments, a leak test is performed by applying a slight gas pressure and checking that the pressure in the core holder is maintained for a period of time.

d. The core holder is placed in the second chamber and leveled.

In cases where CT scanning is performed, the second chamber is filled with water. Water is introduced to the open bottom face of the core and the progress of the

imbibition front monitored with frequent CT-scans. Figure 2.5 shows how the core is placed inside the core holder in chamber 1.

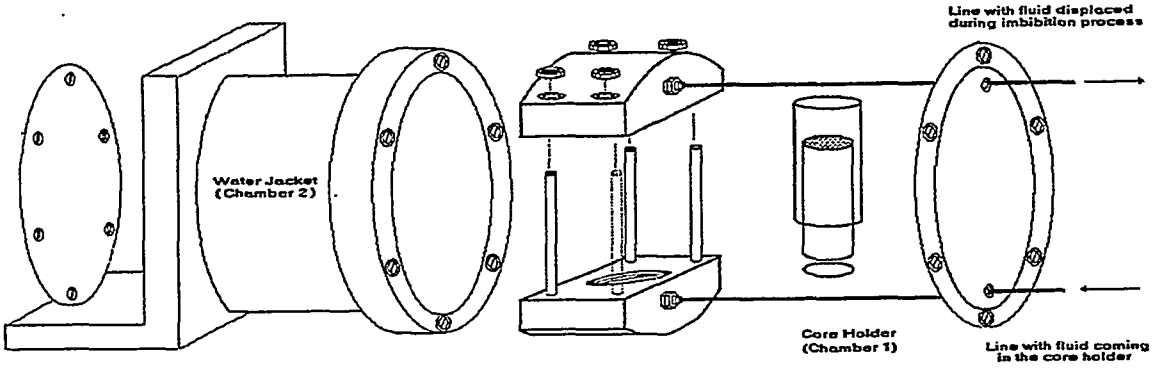

Fig. 2.5 Details of the placement of the core inside the water jacket or core holder

Since imbibition is spontaneous, care was taken to maintain the water level in the core holder so that it just contacts the rock base. The data acquisition system for the balance is started. Once the imbibition begins, the weight of the water reservoir is recorded every 10 seconds. The gain of weight in the core is computed directly by the decrease of weight measured in the tank containing the water. The reference weight corresponds to time equal to zero in which the supply tubing is filled with water and the water-air interface is just below the bottom face of the core.

In the case where CT-Scanning is performed, dry images of the core are taken to obtain the reference dry core CT-values. Once imbibition has begun, scanning is performed every 50 seconds for the first 5 minutes. Afterwards the intervals between the images are longer since the change of saturation in the core becomes slower with time.

The data acquisition process is stopped when changes in the weight are no longer observed. Also, constant water saturation is verified by measuring the average CT-number and standard deviation in the image of the core and then verifying that it is the same from one scan to another. In order to have a reference wet image of the core, a final scan is conducted at least 12 hours later. After spontaneous imbibition is complete, water is sometimes pumped through the core to ensure 100% water saturation.

2.2.3 Data Processing

Once the weight-gain data is collected during the spontaneous imbibition process, it is converted into weight imbibed into the core and a linear regression is performed to obtain the slope of the resulting straight line. This correlates the weight gain of the core to the square root of time. The linear regression was performed using a code written in C++ (given in Appendix A), that reads the raw data stored in a file, transforms it into a two dimensional array containing the square root of time and the weight gained corresponding to that specific time. This array is manipulated by the main linear regression function which calculates the regression coefficients and regression statistics such as variance and the coefficient of determination that indicates how well the linear expression found fits the actual data.

The CT-number related calculations, the map of porosity, and the saturation profiles are obtained using the method of subtraction of images of raw CT data described in Eqs. 1.8 and 1.9.

2.3 Results

In this section, we first present and summarize weight gain as a function of time. Then, we discuss the results obtained when we apply a scaling group to both the weight gain and elapsed time for each rock type. Finally, the corresponding CT-images of the imbibition process are given.

2.3.1 Weight Gain vs Square Root of Time

Data obtained from the imbibition experiments for the different cores were converted into the weight of water imbibed as a function of square root of time in order to measure the rate of change of water saturation in the core. The results are summarized in Figs. 2.6-2.9 and in Table 2.2.

Table 2.2 Results Obtained for Spontaneous Imbibition in Different Experiments

Core	Rock Type	Slope [1E1 gr/sec$^{0.5}$]	Porosity %	Imbibition Potential[1E3dynes]	Slope/A [1E2gr/sec$^{0.5}$/cm^2]
1	Berea	1.422	15	3.995	3.46
1	Berea	1.488	15	4.448	3.66
1	Berea	1.499	15	5.171	3.93
2	Berea	1.472	15	4.336	3.61
3	Diatomite	4.480	65	5.912	8.77
3	Diatomite	4.331	65	6.146	8.93
4	Chalk	0.605	21	0.385	1.27

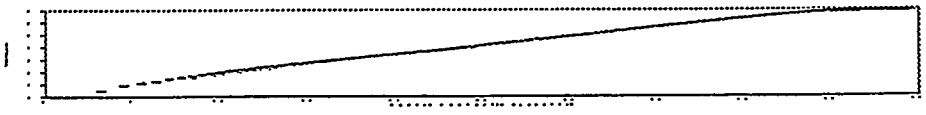

Fig. 2.6. Repeatability tests in Berea sandstone

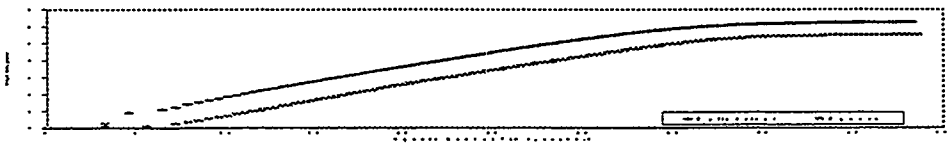

Fig. 2.7 Results for cylindrical and square shaped cores

Figure 2.6 plots the weight gain versus the square root of time for the Berea sandstone. The three different sets of symbols indicate three different experiments. In this case, the weight gain was measured directly by hanging the core from a balance and bringing a beaker of water up until it just touched the bottom of the core, as described in the experimental section and Fig. 2.2. Deviation from linearity in the early time response is explained by the level of the free water surface in contact with the bottom of the core. Because the core is slightly submerged, imbibition is forced and the response is faster than expected. Once the water front passes the free water level, a straight line results. Note that all experimental runs show a straight line with the same slope indicating good reproducibility. Spontaneous imbibition ceases when the water front reaches the end of the core. This time is practically the same for all three cases.

Next, a series of experiments were performed in Berea sandstone cores to confirm that the cross-sectional shape of the cores did not bias our results. Cores with both circular and square cross-sectional areas, as shown in Fig. 2.7, were used. The straight-line portion in both cases has the same slope. The cross-sectional areas were approximately the same, hence the slopes are the same. The difference in the total weight gain and the time for completion of spontaneous imbibition is due to differences in the length of the cores, as shown in Table 2.1. The core with square cross-sectional area did

not imbibe immediately, because the end of the core was not fully submerged in water initially.

These initial experiments with Berea sandstone confirmed that our experimental approach was adequate to collect the data required. Imbibition in diatomite was considered next. Figure 2.8 shows weight gain obtained for the diatomite during two different experiments. All diatomite experiments were conducted in the imbibition cell. Again, there is some deviation from linearity in the initial stages of imbibition. For later times, the response is linear with respect to the square root of time and the slopes are identical. This deviation can be explained by reasons related to the experimental method. Experiments conducted in the imbibition cell also have the possibility that the water level of the tank is not exactly equal to that of the bottom of the core. Forced imbibition could exist for a short time. The second explanation is the filter paper at the bottom of the imbibition cell, which might not saturate uniformly at the beginning of the imbibition process. Thus, imbibition is retarded initially. Interestingly, the water imbibition process is quite rapid despite the low permeability of diatomite. These diatomite samples imbibe water at rates rivaling sandstone.

For comparison, experiments on a low permeability chalk sample were also conducted. Figure 2.9 shows the results. The trend of weight gain is not as smooth as either the sandstone or diatomite case. But, we do observe, overall, a relatively linear response versus the square root of time. Heterogeneities observed during CT-scanning account for the jaggedness of the linear weight gain. These heterogeneities will be discussed further in the next section. Spontaneous imbibition in the chalk is much slower

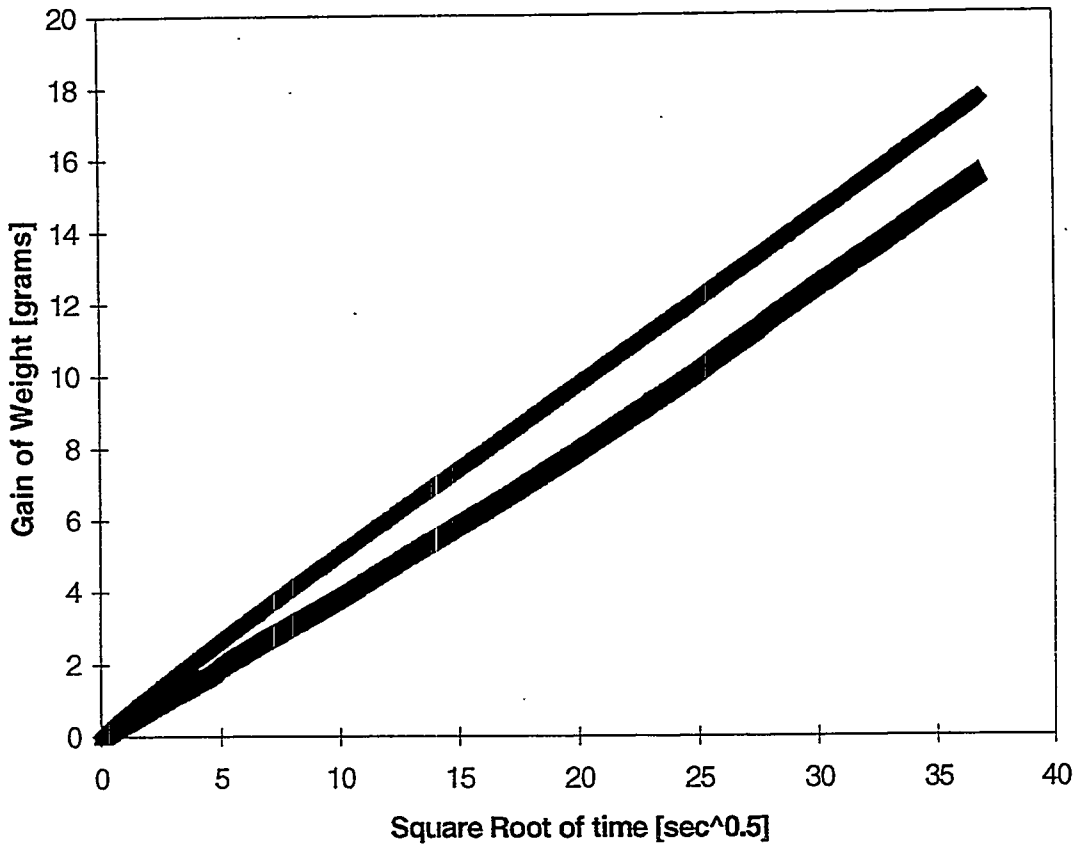

Fig. 2.8 Results obtained for diatomite

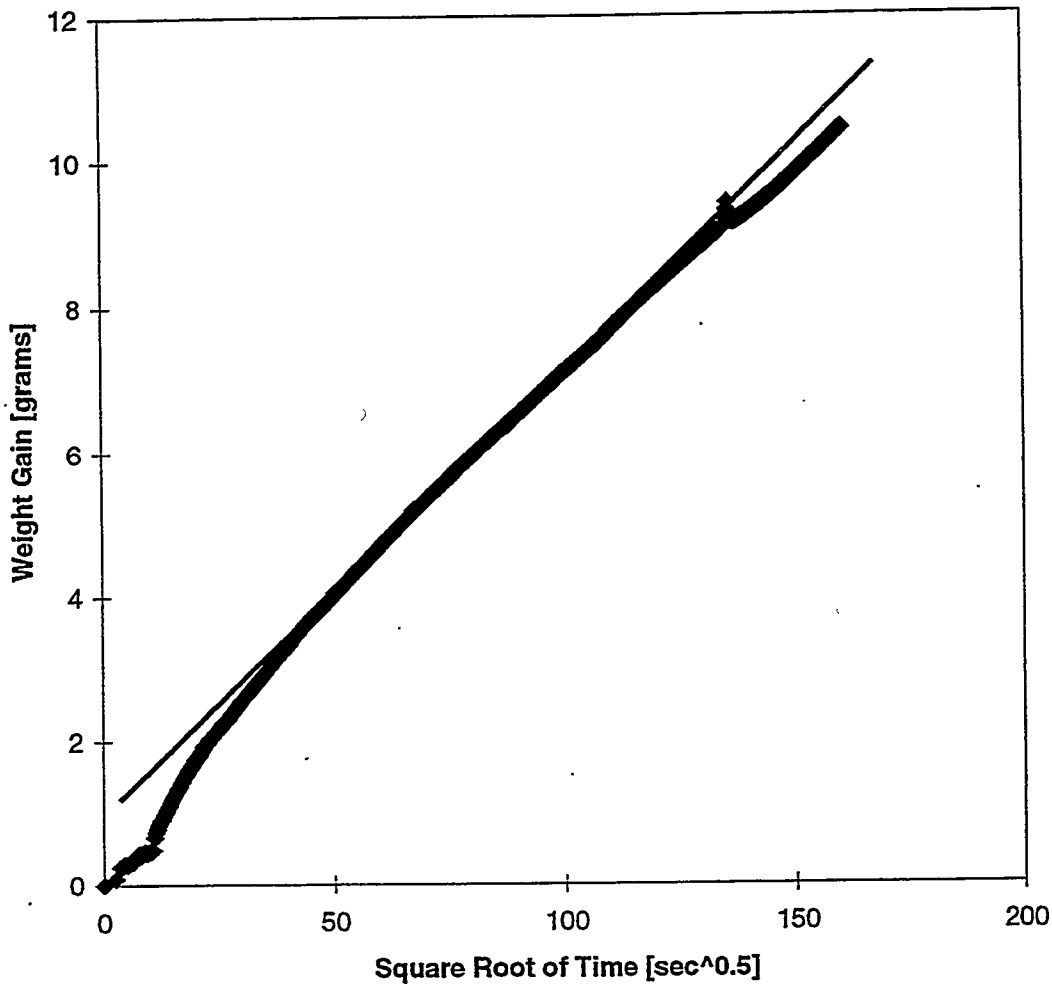

Fig. 2.9 Results obtained for chalk

than in either the Berea sandstone or diatomite, as indicated by the length of time necessary to complete imbibition.

A linear regression was performed on the straight-line portions of Figs. 2.6 to 2.9 to obtain the slope. Table 2.2 shows: (a) the slope, (b) the porosity of the samples obtained by Eq. (1.8), (c) the imbibition potential calculated by Eq. (1.7) and, (d) the slope divided by the cross-sectional area for each experiment. In the case of Berea sandstone with circular cross-sectional area, the three different experiments show similar slope, confirming the repeatability of the method. Also, a similar slope is found for the experiment on square cross-sectional area cores.

The diatomite shows the largest values for slope and imbibition potential. The average imbibition potential for diatomite is 0.0060 dyne, whereas it is only 0.0045 dyne for the sandstone and 0.0038 dyne for the chalk. We find that capillary forces during the spontaneous imbibition process make a contribution to flow that offsets, partially, the low permeability of the diatomite.

2.3.2 Dimensionless Weight Gain

To compare the results of the spontaneous imbibition process, we apply a scaling group to results for the three different types of rocks. Our objective is to verify whether it is appropriate to scale results obtained for sandstone to the case of diatomites. Hence, we attempt to establish if there is a correlation between these types of rock.

In scaling imbibition results for different rocks systems there have been a number of scaling groups proposed (Zhang and Morrow, 1995; Mattax and Kyte, 1962). In this study we define a dimensionless weight gain, m_{wD}, given by

$$m_{wD} = \frac{m_w}{m_{wT}} \tag{2.1}$$

where m_{wT} is the ultimate weight gained during the imbibition process. This term is plotted against a dimensionless time, t', which is defined by

$$t' = t\sqrt{\frac{k}{\phi}}\frac{\sigma}{\mu_w}\frac{1}{L^2} \tag{2.2}$$

where σ is the interfacial tension, and L is the length of the core.

We plot the dimensionless weight gain, m_{wD}, against the dimensionless time, t', for the case of Berea sandstone, diatomite, and chalk. The results are shown in Fig. 2.10. It can be seen that the application of Eqs. 2.1 and 2.2 only scales imbibition results chalk and Berea sandstone. Whereas, in the case of diatomite, the results do not show any correlation between this rock and the other rocks. This fact can be explained by the strong wettability and large capillary pressure that diatomite shows, this produces a very fast imbibition process.

2.3.3 CT-Scanning Results

Porosity maps and the saturation profiles obtained during imbibition for the Berea sandstone, diatomite and chalk are shown in Figs. 2.11-2.13, respectively. Both water

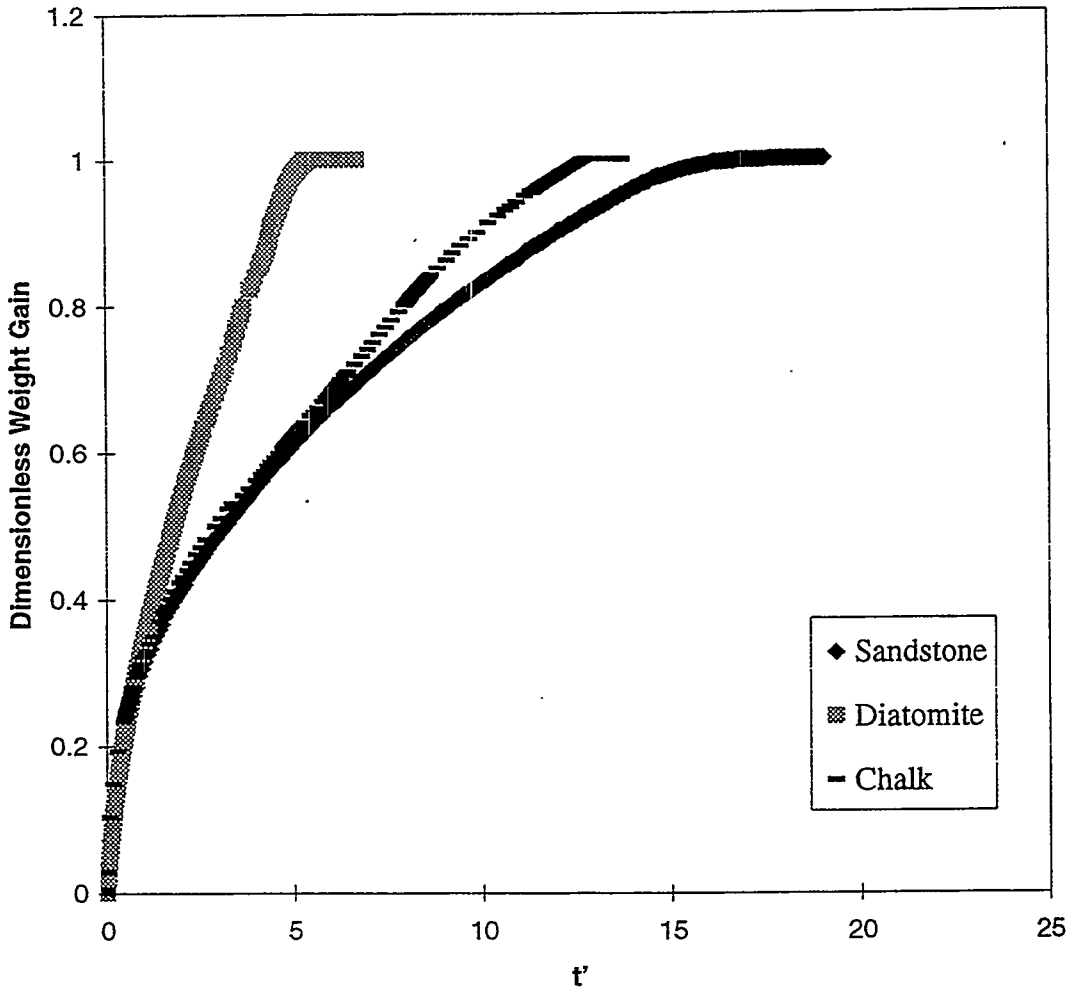

Fig. 2.10 Dimensionless weight gain vs. dimensionless time

saturation and porosity are indicated by gray-scale shading. In the case of saturation, black indicates 0% water and white indicates fully water saturated. Porosity maps are located in the right-hand corner. The shading scale for the porosity images is compressed to highlight heterogeneity, but again dark is small and white is large.

Sandstone porosity ranges from 0.08 to 0.23. The Berea sandstone images in Fig. 2.11 for imbibition show some surprising results. The weight gain data agree with a piston-like assumption, but images of the water displacement front are not truly piston like. Initially, water enters at the center of the core. Intuitively, we expect capillary forces to spread the saturation front laterally as well as upward. However, the front is rounded and centered in the middle of the core (Fig. 2.11 at 200 s). The leading edge of the water front moves through the core maintaining its rounded shape until reaching the core outlet. At about 120 s, the water saturation front does span the cross-section of the core at the inlet. This rear portion of the water front appears to move through the core displacing any remaining mobile gas. Interestingly, the time taken for the rounded water saturation front to span the core (120 s) corresponds roughly with the onset of linear weight gain in Fig. 2.11 (10 $s^{1/2}$).

The porosity map for diatomite shown in Fig. 2.12 indicates that this sample is relatively homogeneous and average porosity is about 65%. Strong capillary forces are evident in the CT images for imbibition in diatomite. Water again enters the core in the center, but it spreads laterally quite rapidly. The water front is sharp and the displacement is clearly piston like. As the front progresses down the core it diffuses somewhat. The water front reaches the end of the core in about 3600 s. These CT images correspond to

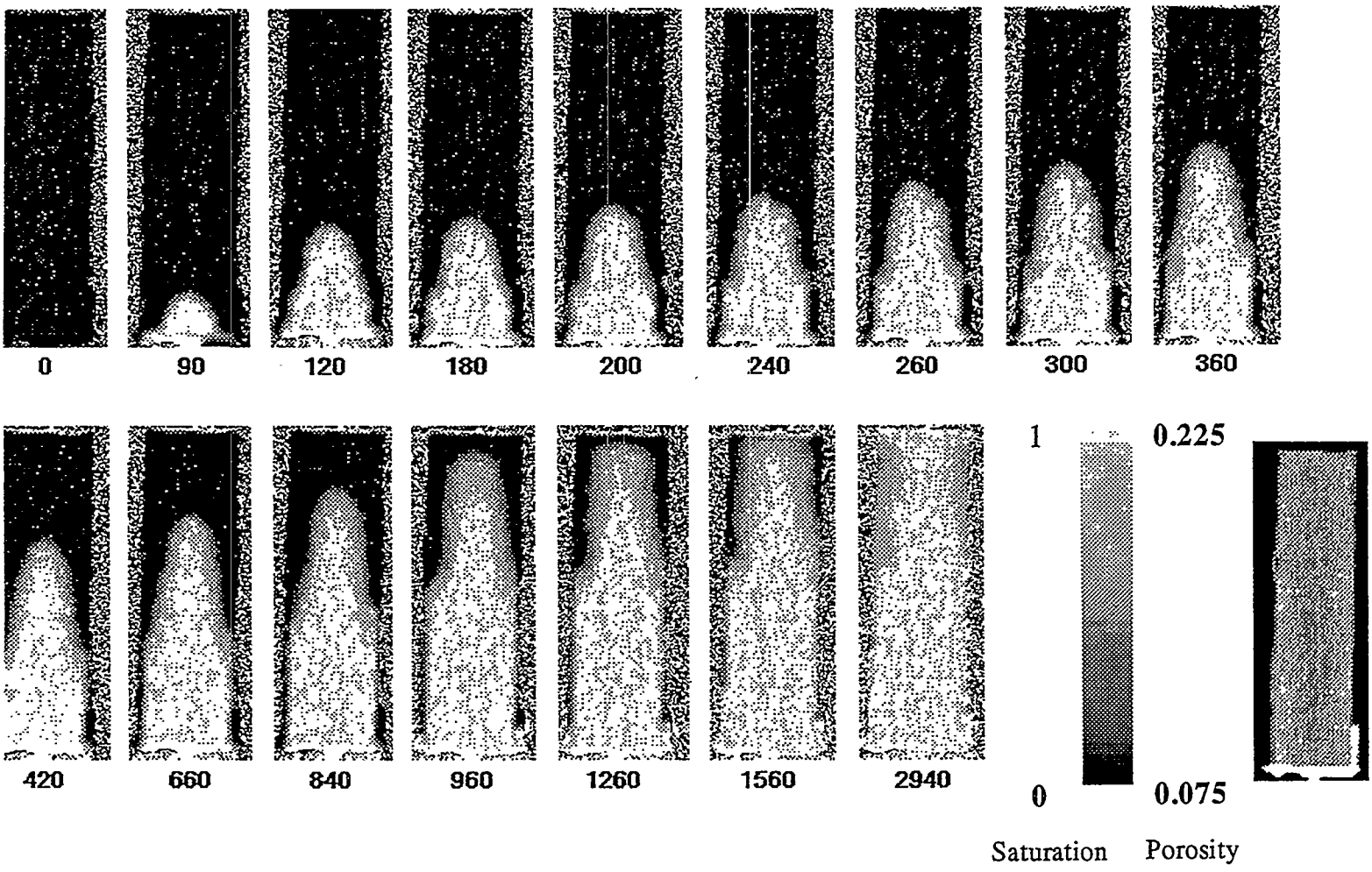

Fig. 2.11 : Images of spontaneous imbibition in Berea sandstone at different times (sec). Water-air system

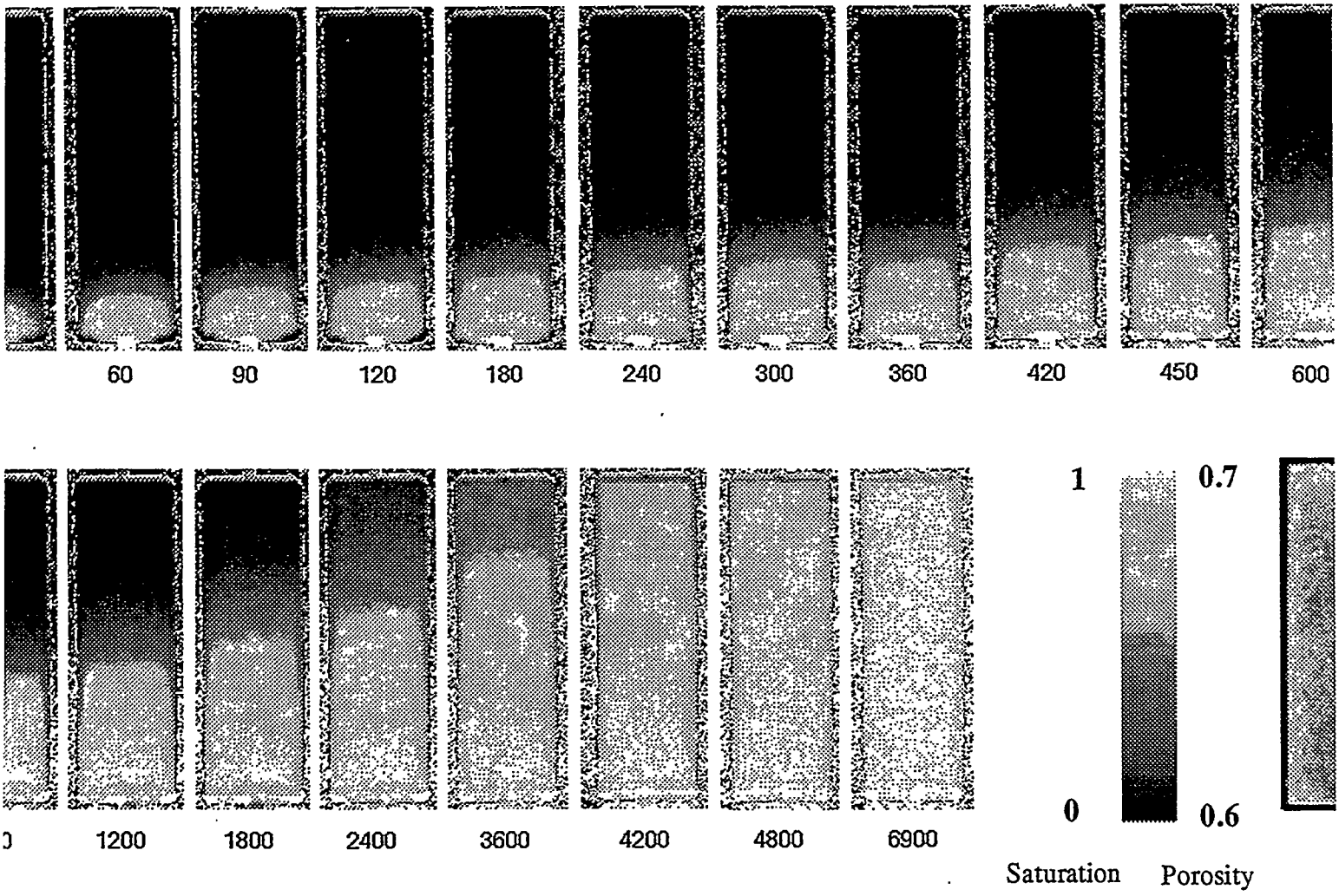

Fig. 2.12 : Images of spontaneous imbibition in diatomite at different times (sec).
Water-air system

the lower curve in Fig. 2.8 that deviated from linearity at short time. Figure 2.12 shows that the saturation front was not one dimensional until roughly 90 s. Hence, the deviation from linearity results from the nonuniform displacement front.

In contrast to the sandstone and diatomite samples, the chalk core contains heterogeneities. These are evident in the porosity map as illustrated in Fig. 2.13. For instance, there is a dark portion, indicating low porosity, on the left-hand side about a quarter of the way up the chalk core. Chalk porosity ranges from 0.15 to 0.25. Like the diatomite, the chalk shows a practically uniform and sharp front at the beginning that becomes more diffuse at later times. It is interesting to note that the heterogeneities fill with water at somewhat different rates. The slow filling of the above mentioned heterogeneity is evident in the saturation images at 300, 540, and 600 s.

A comparison of the time necessary for the spontaneous imbibition to be completed in each type of rock, confirms the weight gain results. Diatomite takes about three times longer than Berea Sandstone, while the chalk takes ten to eleven times. It is important to recall that the pore volume of the diatomite is about five times the pore volume of the Berea sandstone.

2.3.4 Water-Oil Imbibition

Upon construction of an imbibition cell that permits high resolution scanning with minimal CT artifacts, the successful capture of saturation images for water imbibing into an air-filled core, and the excellent repeatability of these experiments, we have turned to water imbibition into diatomite containing oil. First the core is dried as explained above

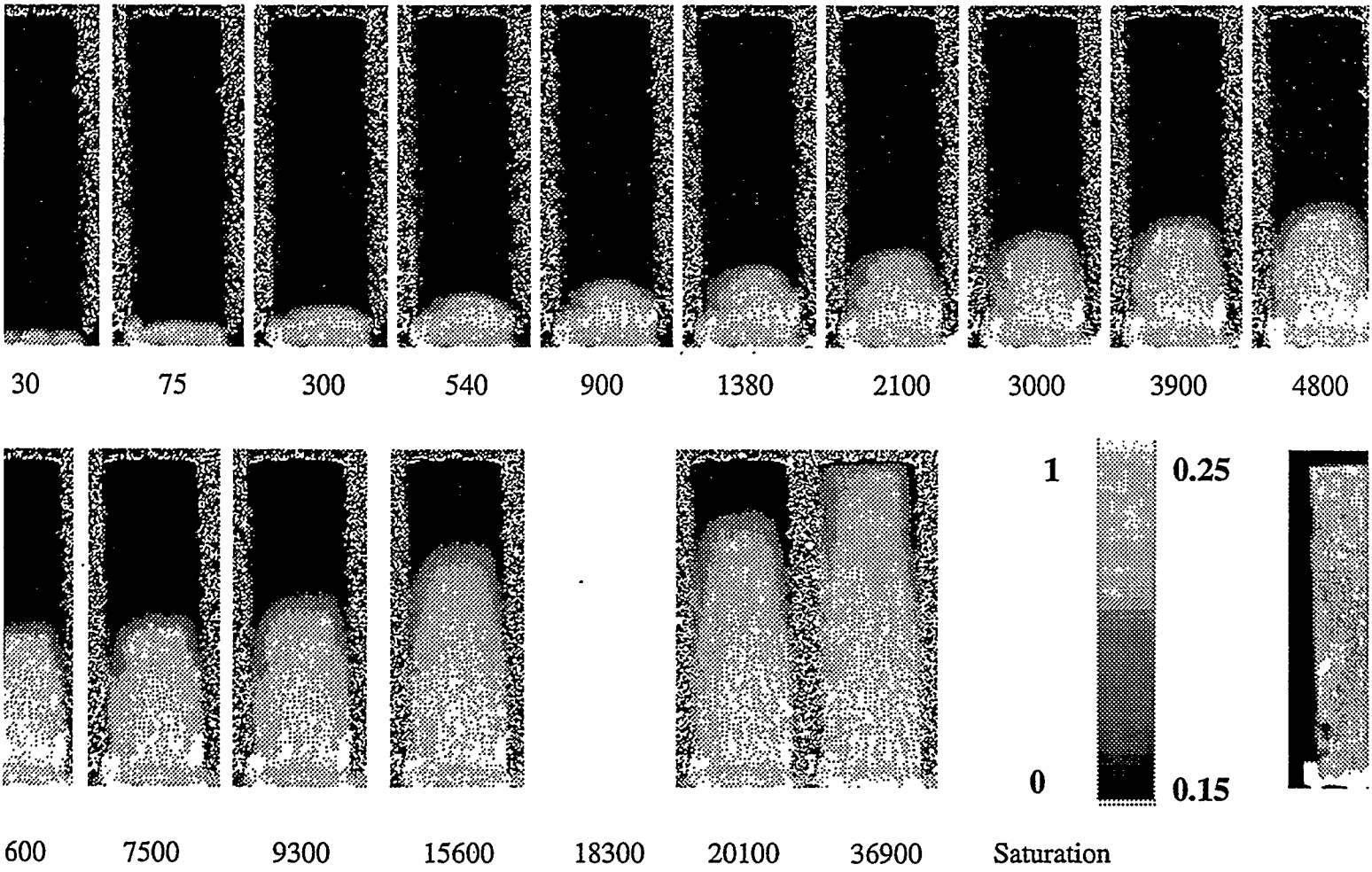

Fig. 2.13 : Images of spontaneous imbibition in chalk at different times (sec) water-air system

and then it is completely saturated with n-decane via vacuum saturation. Oil is purged from the supply lines and replaced with water. The experiment is then conducted in the same manner as the water/air cases. Produced oil exits the top of the core. Some preliminary CT images are shown in Fig. 2.14. From the times associated with each CT image in Fig. 2.14, it is apparent that water imbibition is much slower in the water/oil case than in the water/air case. At 17,460 s in Fig. 2.14 the water/oil front is roughly half of the way up the core, while in Fig. 2.12, imbibition in the water/air system is complete in less than 6900 s. This is expected because the water/oil interfacial tension is lower as are the buoyancy forces. Also, the oil is much more viscous than air and hard to displace. Nevertheless, a strong, sharp displacement front is witnessed and strong capillary effects are evident. Displacement is not as effective in the water/air case. The gray scale shading indicates that the water saturation upstream of the displacement front is about 80%.

Although the experimental setup was designed to promote one-dimensional cocurrent imbibition, there is anecdotal evidence that countercurrent imbibition may have resulted at times due to the strong capillary forces. Periodically, imbibition, as judged from the decrease in weight of the water supply, would cease. In order to restart imbibition, the water reservoir was raised a few centimeters via a laboratory jack until imbibition resumed and then lowered again. Countercurrent imbibition allows oil to exit at the bottom face of the core and this oil could impede water flow. Applying a slight amount of hydraulic head was be sufficient to disturb the system and reinitiate water flow.

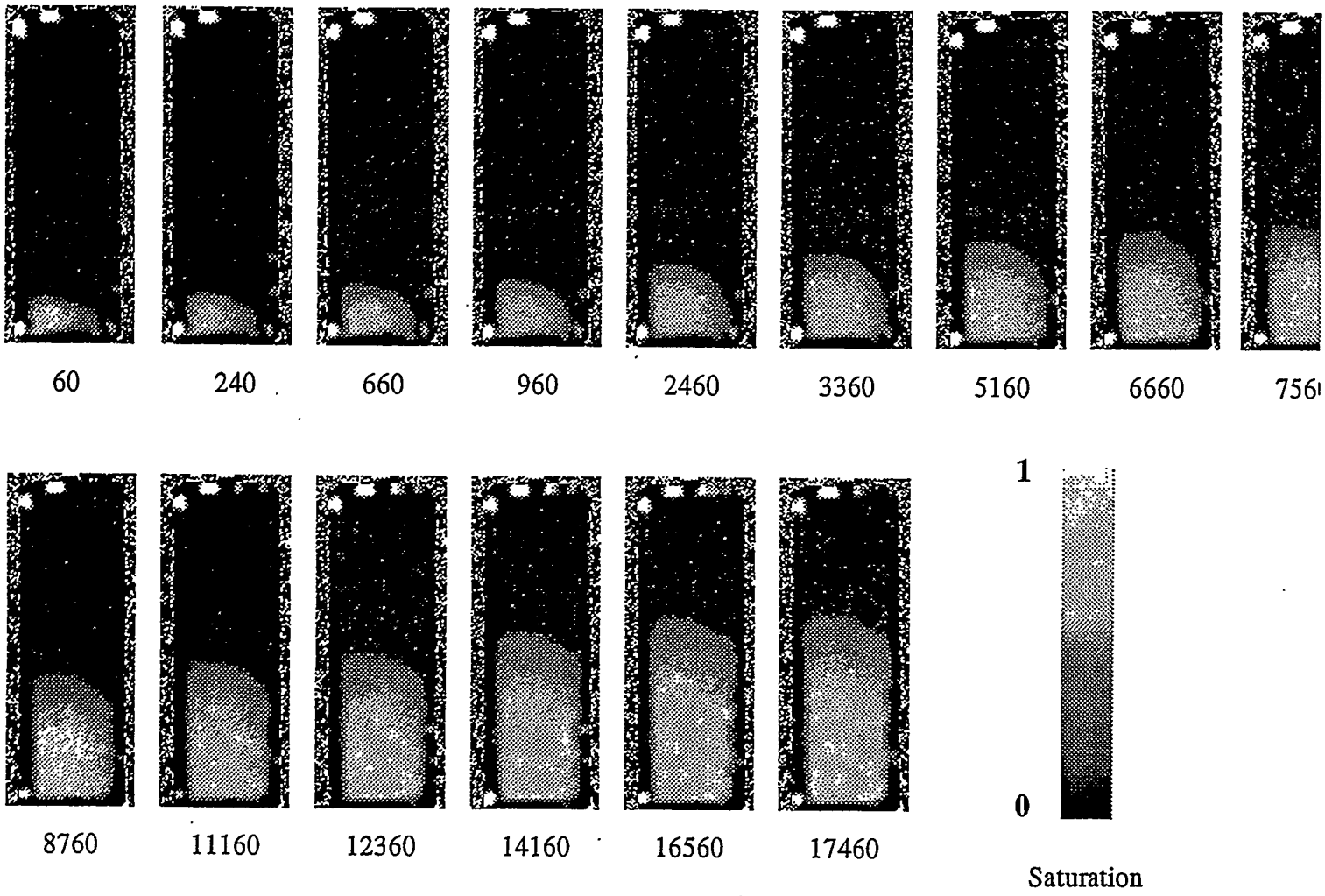

Fig. 2.14 : Images of spontaneous imbibition in diatomite at different times (sec). Water-oil system

2.4 Discussion

The simple water displacing air experiments provide some insight into the capillary pressure characteristics of diatomite. Denote the imbibition potential by *IP* and take the ratio of diatomite *IP* to sandstone:

$$\frac{IP_d}{IP_s} = \frac{(P_c k_w S_w)_d}{(P_c k_w S_w)_s} \tag{2.3}$$

where the subscripts d and s refer to diatomite and sandstone, respectively. Using average values from Table 2.2, this quantity is 2.4 indicating the strong tendency of diatomite to imbibe water. From Figs. 2.11 and 2.12, we judge that the water saturation upstream of the saturation front is about 1. So, the ratio of saturations in Eq. 2.3 is about 1. Next, we replace P_c with the appropriate Leverett J-function:

$$P_c = \sigma\left(\frac{\phi}{k}\right)^{1/2} J(S_w) \tag{2.4}$$

for water-wet rocks. In Eq. 2.4, σ is the air-water interfacial tension and $J(S_w)$ is the Leverett J-function (Leverett, 1941). Upon some rearrangement

$$\frac{IP_d}{IP_s} = \left(\frac{k_d}{k_s}\right)^{1/2}\left(\frac{\phi_d}{\phi_s}\right)^{1/2}\left(\frac{J_d(S_w)}{J_s(S_w)}\right) > 1 \tag{2.5}$$

Equation (2.5) teaches us about the magnitude of the J-function for diatomite. The first term in parentheses on the right is clearly less than 1 because diatomite is less permeable than sandstone. With typical sandstone (100 to 1000 *md*) and diatomite (0.1 to 10 *md*) permeabilities, k_d / k_s, might range from 0.1 to 1E-4. Table 2.2 shows that the diatomite

samples are roughly 4 times as porous as the sandstone. For 2.5 to be greater than 1, J_d / J_s must be greater than 1. This explains, in part, why the relatively impermeable diatomite imbibes strongly when the rock is initially filled with air.

Another interesting aspect of these experiments is the very low trapped gas saturation. For instance, Fig. 2.12 at 4800 s shows water saturation in excess of 95% shortly after breakthrough. The strong capillary forces and the small pore throat to body aspect ratio of diatomite suggests much snap-off and trapped gas. However, for snap-off to occur, pore corners and crevices must fill with wetting liquid and sufficient liquid for snap-off must accumulate at pore throats before the pore is filled completely by the advancing imbibition front. We speculate that trapped gas saturation is low because the advancing front fills pores with water at least as rapidly as pore corners fill with water. Indeed, recent pore-level network modeling of imbibition shows that in the absence of flow in pore corners the displacement pattern is a flat front with little or no trapping of the nonwetting phase (Blunt and Scher, 1995).

2.5 Conclusions

An experimental apparatus and method to permit the collection of data and CT images during spontaneous imbibition into an air or oil-filled core was designed. The samples examined were Berea sandstone, diatomite and chalk, which allowed the study and comparison of the contribution of porosity, permeability, and capillary forces during imbibition. Several tests were performed and they confirmed the repeatability of the

method. The water/air system was examined extensively. It was confirmed that different core cross-sectional areas did not bias results.

CT imaging of the imbibition process permitted not only the observation of the advance of the water front into the cores, but explains the observed trends in weight gain as a function of time. Images obtained for diatomites and chalk show an homogeneous and piston-like water front during the process. Results for sandstone showed good agreement with previous work (Handy, 1960; Garg *et al.*, 1996; Babadagli and Ershaghi, 1992) and permitted the comparison of imbibition potential for different types of rocks. Application of scaling group analysis permitted the study of the poor correlation between imbibition results for diatomite and the two other types of rocks. In impermeable diatomite, capillary forces result in a strong imbibition potential for water. However, the rate of imbibition in oil-filled systems appears to be slow. This work is a stepping stone to a more complete study of spontaneous imbibition in water/oil systems.

3 SIMULATION AND HISTORY MATCHING OF EXPERIMENTAL RESULTS

3.1 Introduction

In the previous chapters we presented the importance of studying the properties of diatomites and the results of experiments performed in different rocks such as sandstone,chalk and diatomites. We were able to compare the behavior of diatomaceous rocks and make some conclusions about the high imbibition potential and its relation to strong capillary forces in this rock.

In defining imbibition potential we combined the effective permeability of the water phase (which is the product of the permeability and relative permeability of the water), the capillary pressure, and water saturation into a single parameter. The three parameters are interrelated. The capillary pressure and permeability depend on the water saturation and they also depend on the rock wettability.

In this section, we study in more detail the properties of the rock and the effect that each of these properties have on the process of spontaneous imbibition. The method we followed here consisted of extracting relative permeability and capillary pressure from the experimental data and matching with a numerical simulator the experimental results obtained for the water-air system in diatomite. We match the gain of weight

versus the square root of time, and the saturation profile at different times. The saturation profiles are obtained from the saturation numbers given in the CT images.

With the history matching, we not only attempt to understand the mechanisms involved in the process of spontaneous imbibition in low-permeability rocks but also to estimate some of petrophysical properties of this rock such as relative permeability and capillary pressure by using a new parameter estimation method. These properties are essential input for the prediction of reservoir performance.

3.2 Estimation of Relative Permeability and Capillary Pressure Curves

3.2.1 Literature Review

Before we describe in detail the method proposed to estimate the relative permeability and capillary pressure, we present a brief review of the effect of these parameters on the displacement and some methods used to estimate them.

Relative Permeability

Relative permeability is "a direct measure of the ability of the porous system to conduct one fluid when one or more fluids are present" (Craig, 1971). These flow properties are the composite effect of pore geometry, wettability, fluid distribution, ad saturation history" Relative permeability curves are critical in any calculations of displacement in porous media. In the literature many methods are mentioned for the

estimation of relative permeabilities on the basis of displacement experiments (Baticky *et al.*, 1980; Kerig and Watson, 1987; Lai and Brandt, 1988; Watson *et al.*, 1988). One disadvantage of these methods is that capillary effects are often neglected. Sigmund and McCaffery (1979) used an implicit method, where they performed non-linear regression assuming that the relative permeability curve of the water behaves according to a the power-law model. We will show that this assumption can lead to significant errors.

Capillary Pressure

Capillary pressure is the difference in pressure that exists between two fluids across the interface that separates them,

$$p_c = p_{nw} - p_w \tag{3.1}$$

where, the subscripts nw and w refer to non-wetting and wetting phase, respectively. The value of the capillary pressure is determined by the interfacial tension between the two fluids, and it is inversely proportional to the average radius of curvature (Bentsen, 1978). Thus, the capillary pressure increases as the pore become smaller or the wetting phase is more strongly wetting.

Currently, during the evaluation of relative permeability curves, the common practice is to conduct coreflooding experiments so that the capillary pressure gradient in the direction of the flow is small compared with the imposed pressure gradient. In rocks such as diatomite, in which it has been demonstrated that capillary forces play an important role during the waterflooding process, it is important to monitor the effect of capillary forces and wettability during the displacement. In general, dynamically

measured capillary pressure properties not only indicate strong, weak, intermediate or mixed wettability but also provide an idea about the relative permeability data from displacement experiments.

3.2.2 Method used for Matching the Slope and Saturation Profile

In the parameter-estimation method, parameter estimates are chosen so as to minimize a weighted sum of squared differences between the measured data and the values calculated from a mathematical model of the experiment . The measured data used are the linear correlation between the water imbibed and the square root of time, and the saturation profiles for the different times which have been obtained from converting the CT images to pixel numbers as shown in Fig. 3.1.

The mathematical model used in this study is given by the expression:

$$u_w = \frac{k k_{rw}}{\mu_w} \frac{dp_c}{dx} \tag{3.2}$$

This is the differential form of Eq.(1.3) in where we have neglected the effect of gravity forces and assumed that the pressure gradient in the gaseous phase is minimal. Substituting $u_w = \phi v_w = \phi \frac{dx}{dt}$ in Eq. (3.2) results in

$$\phi \frac{dx}{dt} = \frac{k k_{rw}}{\mu_w} \frac{dp_c}{dx} \tag{3.3}$$

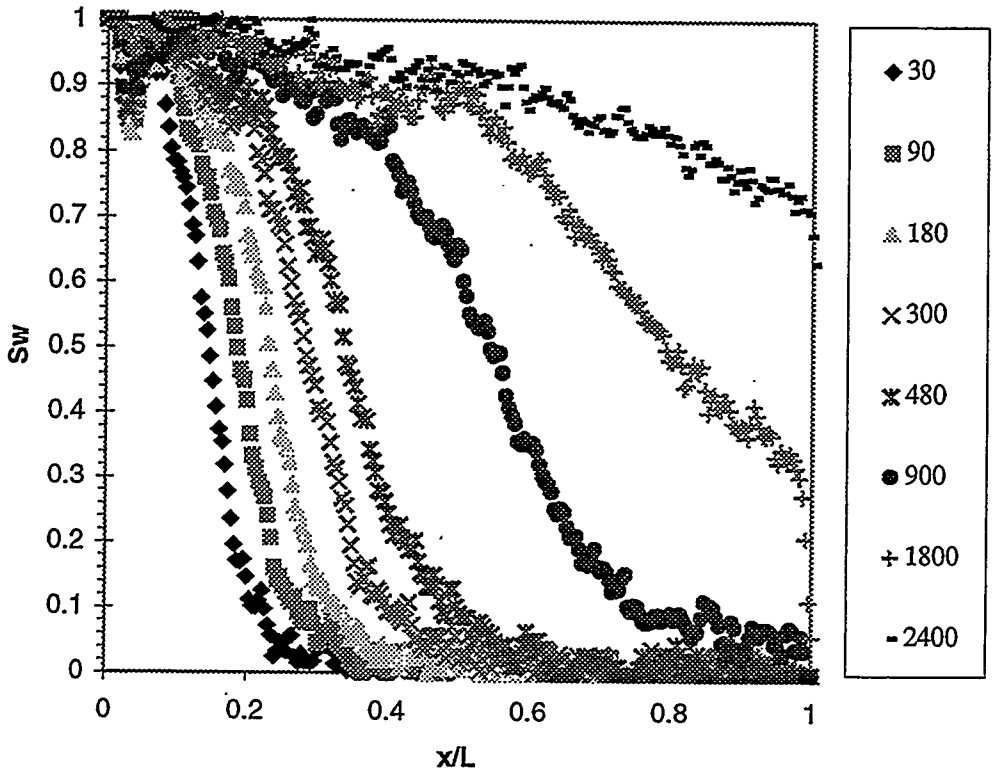

Fig. 3.1 Saturation profiles obtained during the CT-Scan process at different times [sec]

Since the capillary pressure is a function of the saturation and the saturation profile is available, we express $\frac{dp_c}{dx}$ as $\frac{dp_c}{dS_w}\frac{dS_w}{dx}$, and Eq. (3.3) becomes

$$\frac{dx}{dt} = \frac{kk_{rw}}{\mu_w \phi}\frac{dp_c}{dS_w}\frac{dS_w}{dx} \tag{3.4}$$

for a given time and saturation.

From the experimental results we can see that there is a linear relationship between the position of the front for a given saturation and the square root of time. Therefore we introduce a new variable, τ ,

$$\tau = \sqrt{t} \tag{3.5}$$

which permits us to express the relation in Eq. 3.4 in terms of the slope obtained from plotting the position front vs. square root of time for the different saturations. By introducing this new variable in the differential equation, we have the following objective function $F(S_w)$,

$$F(S_w) = \frac{1}{2\sqrt{t}}\frac{dx}{d\tau}\bigg|_{Sw,t} - \frac{kk_{rw}}{\mu_w \phi}\frac{dp_c}{dS_w}\frac{dSw}{dx}\bigg|_{Sw,t} = 0 \tag{3.6}$$

In this function we have that the porosity and permeability are known and the differential terms are found from the plot of saturation profiles, the two unknown terms terms, $\frac{dx}{d\tau}$ and $\frac{dp_c}{dS_w}$, are the relative permeability and the derivative of capillary pressure. By using a non-linear regression method, we obtain these two terms with the following procedure:

1. We assume a model for the capillary pressure, in this case our guess was given by $p_c = -3\ln(S_w)$. Having the analytical derivative for this curve, we fix the saturation and solve for an unique k_{rw} at that specific saturation for different time. This procedure is repeated for different saturations in the range from 0 to 1.
2. We plot k_{rw} vs S_w and this would give us a first iteration for the relative permeability curve.
3. We fix the relative permeability curve, and we solve this time for dp_c / dS_w at specific saturation for different times. We repeat this procedure for the different saturations.
4. By integrating the term dp_c / dS_w, we obtain a new capillary pressure curve, that we use to repeat the procedure described in Step 1.

We simulate the imbibition process and compare not only the slope of the weight gained in the core against the square root of time, but the saturation profiles at different times. The former comparison allows us to find the permeability given the capillary pressure curve as is normally performed in most history matching methods. The latter allows us to fix the shape of the front. The shape of the capillary pressure curve plays an important role in the displacement as will be discussed later.

3.3 Numerical Simulator and Model Input

The numerical simulator used to compute gain weight and saturation history was ECLIPSE 100. It is a fully-implicit, black-oil simulator written in FORTRAN 77 and developed by Geoquest, Schlumberger.

The core was modeled in radial block-center coordinates as shown in Fig. 3.2, with 102 cells in the z-direction, and one cell in the radial and angular coordinates so that the flow is one dimensional. The top and bottom cells, emulating the water source (bottom) and open atmosphere conditions (top), have different volume and properties from the inner cells. The remaining cells have the petrophysical properties of the core (see Fig. 3.2).

The experiment is modeled as a water-gas system, the petrophysical and fluids properties are shown in Table 3.1. The porosity input is the one measured in the laboratory by the method of subtraction of images. The permeability was measured in the laboratory using a Ruska permeameter. The relative permeability of the air is assumed to follow the power law with exponent 2. It is assumed that there is not initial water saturation nor residual non-wetting phase saturation ($S_{wi} = S_{nwr} = 0$).

The capillary pressure and water relative permeability curve for the core were not available and they will be the parameters to be determined by the method described in the following section.

Table 3.1: Petrophysical and Fluid Properties Input in the Numerical Simulation

Core	
Porosity	0.65
Permeability[md]	15.8
Compressibility[1/atm]	5E-5
Fluids	
Water	
Viscosity [cp]	1.0
Density[g/cm^3]	1.0
Compressibility[1/atm]	5E-5
d(Viscosity)/dp [cp/atm]	0.0
Air	
Viscosity[cp]	1.812E-2
Density[gr/cm^3]	1.0
k_{rg}	$(1\text{-}Sw)^2$
P_{cg} [atm]	0.0

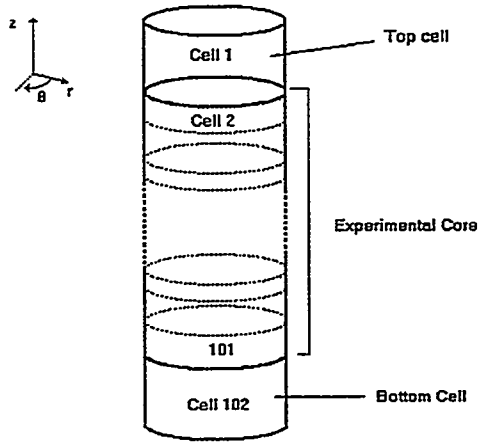

Fig.3.2 Scheme of the core input in the numerical simulation

3.4 Results

In this section, we divide the discussion in two parts. The first part is dedicated to study the effects of assumptions of power-law model for the relative permeability curve and logarithmic model for the capillary pressure. We present results obtained from the numerical simulation so we can compare it to the experimental profile. This will allow us to discuss in detail the influence of the shape of both curves on the saturation profile. Afterwards, we present the results obtained when the parameter-estimation method described in the previous section is performed.

3.4.1. Weight Gain

In the literature, the non-uniqueness of the solution obtained for history matching has been commented upon extensively. Indeed, we observed that there are different combinations of these two parameters that match the linear relationship between the weight gained and the square root of time. As a first approach for matching the experimental results, we found the relative permeability curve for different fixed capillary pressure curves, assuming that the relative permeability curve follows the power-law model, $k_{rw} = AS_w^B$, and the capillary pressure is given by the natural logarithmic model $p_c = -p_{co}\ln(S_w)$. We fix the capillary pressure parameter p_{co} and find different combinations of the fitting parameters for the relative permeability curve, A and B, so that the experimental weight-gain slope is matched. We compare five different tests in Table 3.2. In tests 1,2, and 3, the value of the capillary pressure parameter p_{co} was fixed at a value of 3 atm. This value was selected according to experimental measurements of capillary pressure performed in diatomite cores. We see

that the values obtained for the coefficient A increases when exponent B is increased. This is due to the fact that when the exponent B is larger, the curve shows lower values for a larger range of the water saturations. This results in larger values for $S_w = 1$ in the relative permeability curve. On the another hand, if we compare the saturation profiles shown in Figs. 3.3 and 3.4 for the case of exponent $B = 2$ and $B = 3$, respectively, we notice that as B increases the saturation profile shows a sharper front, approaching piston-like behavior.

Table 3.2 Results of the Different Combinations of Parameters in the Models of Capillary Pressure, $pc = -p_{co} \ln(S_w)$, and Relative Permeability Curve, $k_{rw} = AS_w^B$.

Test #	P_{co}	A	B
1	3	0.45	2
2	3	0.5	2.5
3	3	0.6	3
4	2.5	0.65	3
5	3.5	0.55	3

Fixing the value of exponent $B = 3$, we can see that as we decrease the value of the capillary pressure parameter, p_{co}, the relative permeability coefficient, A, increases. This is explained by the fact that, if the difference between the two phases decreases, the driving forces also decreases, this must be compensated by a larger value in the conductivity of the water phase.

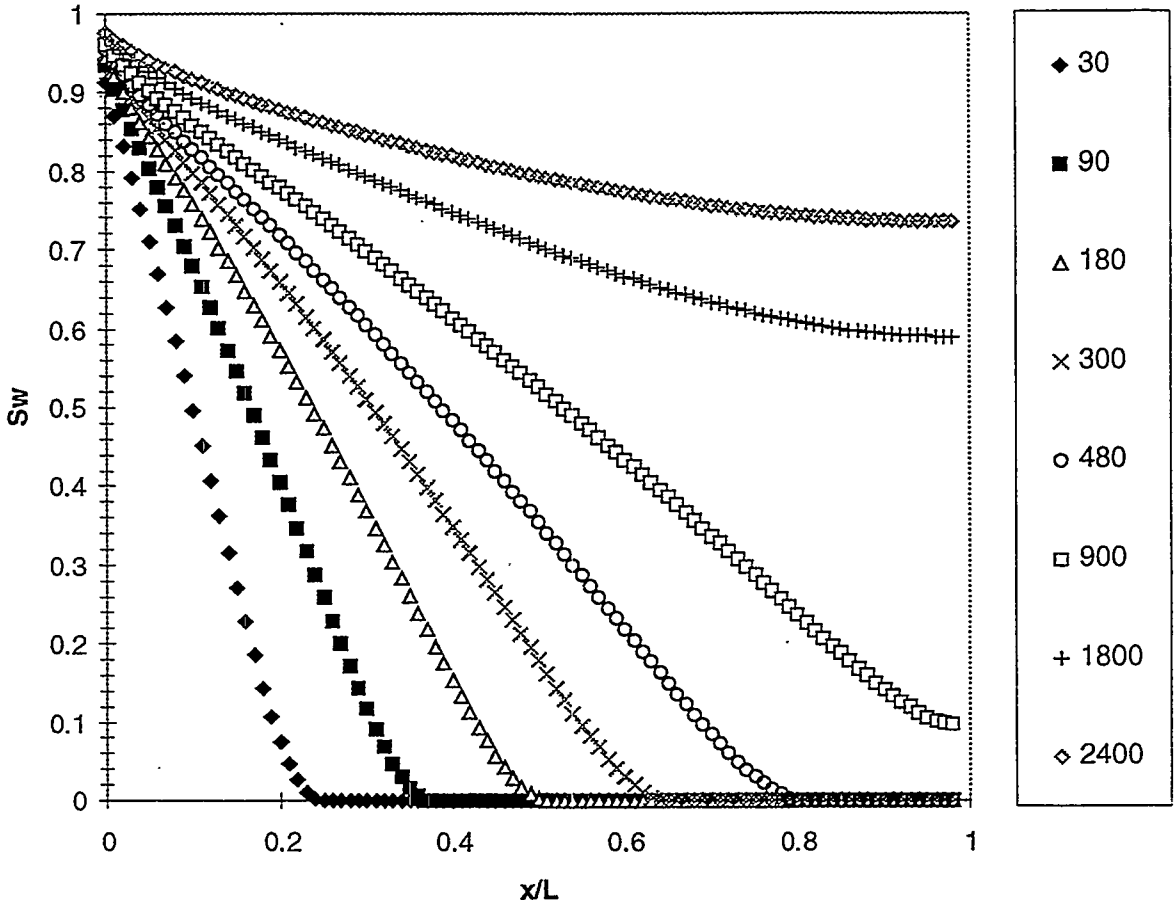

Fig.3.3 : Normalized saturation profile for logarithmic model in the capillary pressure, $P_c = -3\ln(S_w)$

$k_{rw} = 0.45 S_w^2$.

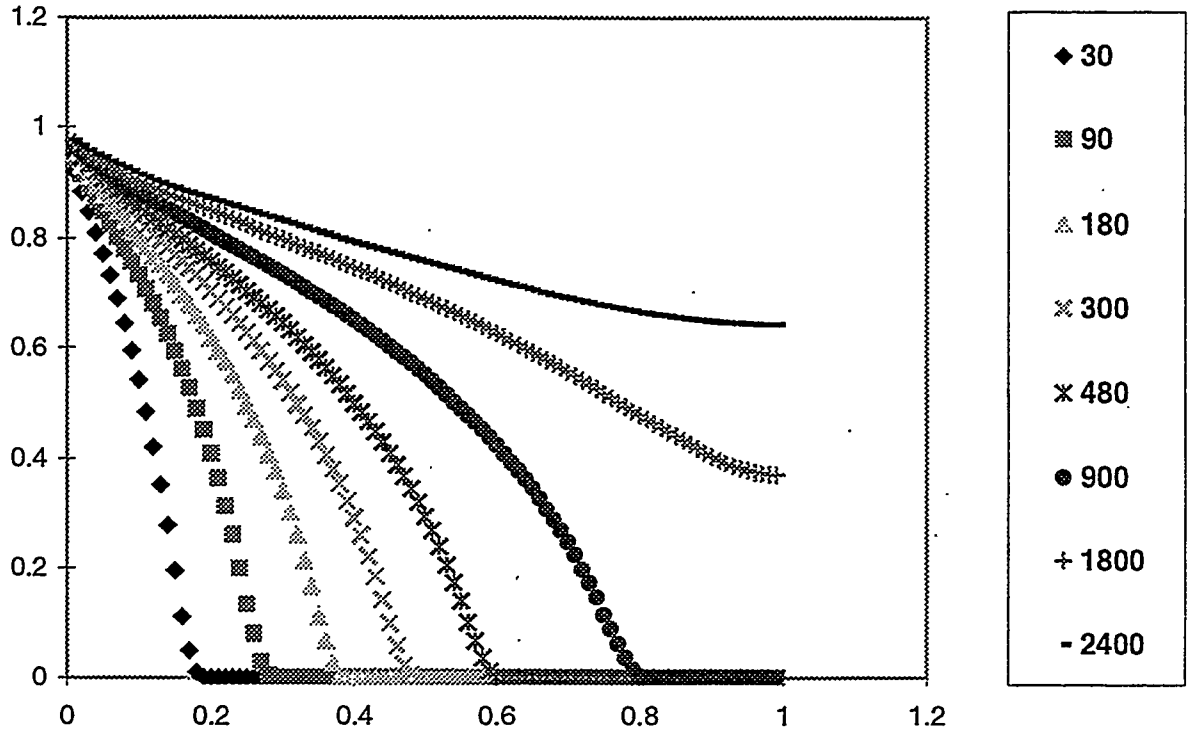

Fig.3.4 : Normalized saturation profile for logarithmic model in the capillary pressure, $P_c = -3\ln(S_w)$

$K_{rw} = 0.55 S_w^3$

On the other hand, when we look at the relative permeability curve, we see that in order to attain a piston-like behavior we should increase the value of the exponent B in the power-law model, this will lead to larger coefficient, A. In contrast, we have that in strongly water-wet systems the effective water permeability at the residual non-wetting saturation is very low and it is much less that the air permeability at the initial water saturation (Anderson, 1987). Although these results matched the weight gain, they do not match the experimental saturation profiles.

3.4.2. Saturation Profiles

In order to obtain the capillary pressure and relative permeability curves that match both the weight gain and the saturation profiles, we used the parameter-estimation model previously described. Matching the saturation profile constrains the solution considerably.

First we plot the displacement *versus* the square root of time for different saturations. Figure 3.5 shows the plots obtained for different saturations. We perform a linear regression for each S_w. The slope, λ, obtained is the velocity of the saturation. It is important to mention that, because experimental results show a retardation in the imbibition process at earlier times, this retardation causes the y -intercept of this line to be different from zero. The y-intercept, ε, found by the linear fit, determines the time shift in the term $dx/d\tau$ in Eq. 3.6 for every saturation. The coefficients found by linear fits for different saturation are shown in Table 3.3. We can see in Fig. 3.5 and Table 3.3 how the slope, λ, decreases with saturation.

Table 3.3. Coefficients for linear fit, $\lambda t^{0.5} + \varepsilon$ for different saturations

S_w	λ[1E+02 $sec^{-0.5}$]	ε [1E+02]
0.1	1.80	9.49
0.2	1.50	9.29
0.3	1.28	10.03
0.4	1.23	8.57
0.5	1.21	7.2
0.6	1.13	6.8
0.7	1.01	6.19
0.8	0.92	4.16
0.9	0.49	3.56

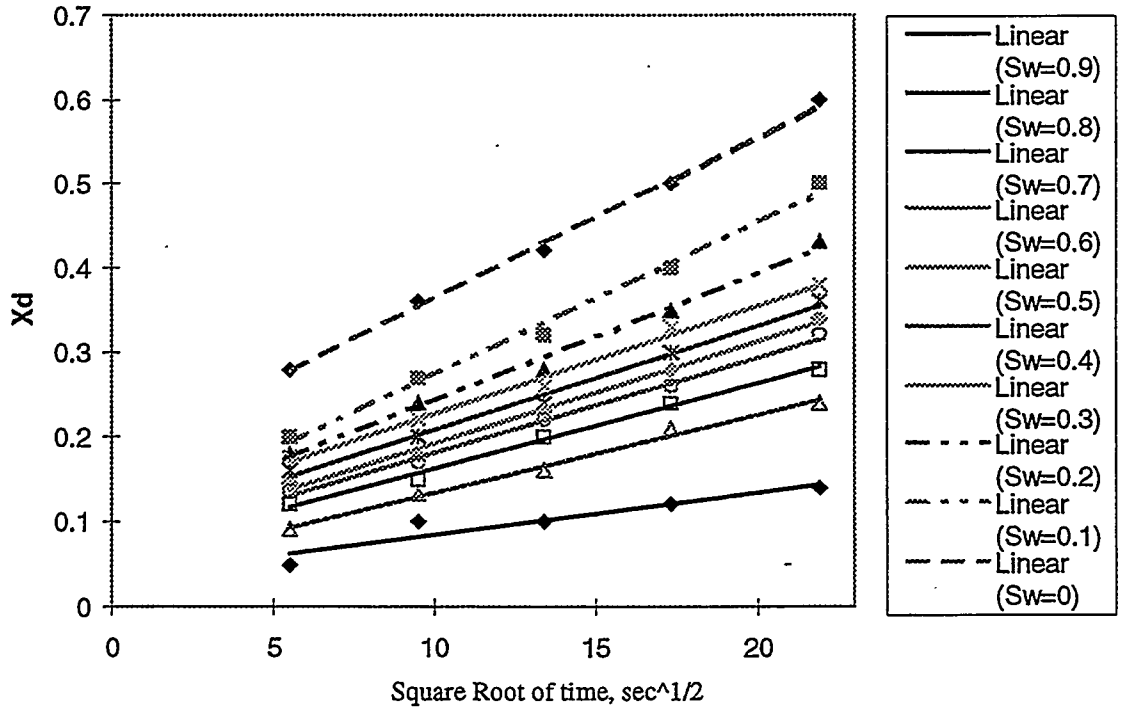

Fig. 3.5 Plot of position vs the square root of time for $S_w = 0.1$

With the values obtained from the CT data, and using Eq. (3.6) as the objective function in the parameter-estimation technique, we found the water relative permeability and capillary pressure curves shown in Figs. 3.6 and 3.7, respectively. We see that the relative permeability curve does not follow the power-law model, and the value at the residual non-wetting saturation is much lower than those obtained for the case of power-law model. Regarding the capillary pressure curve, it does not have a logarithmic-like behavior. It shows high pressure at $S_w = 0$, however this value is close to measurements performed in the laboratory. It is important to mention that the most critical points to determine by this technique are the points corresponding to the extreme values of $S_w = 0$ and $S_w = 1.0$.

Once we have the capillary pressure curve, we compute the Leverett J-function which characterizes and permits the comparison of diatomite with different sands (Bear, 1988. The J-Leverett J-function for water-wet media is defined as

$$J(S_w) = \frac{p_c}{\sigma}\sqrt{\frac{k}{\phi}} \tag{3.7}$$

The Leverett J-function obtained for diatomites via history matching is shown in Fig. 3.8. It can noted that the high values obtained for the capillary pressure compensate for the low permeability of the diatomite during displacements. This results in higher values in the Leverett J-function in water saturation ranges between 0.2 and 0.8 compared to the Leverett J-function for sands. This is expected from the order of magnitude analysis in Section 2.4.

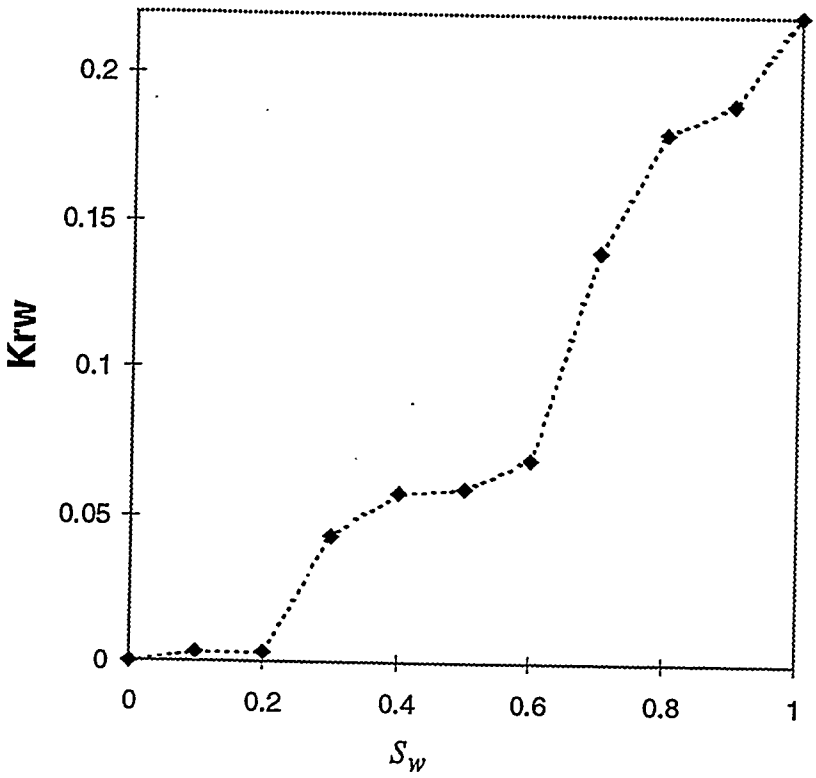

Fig. 3.6 Relative permeability curve

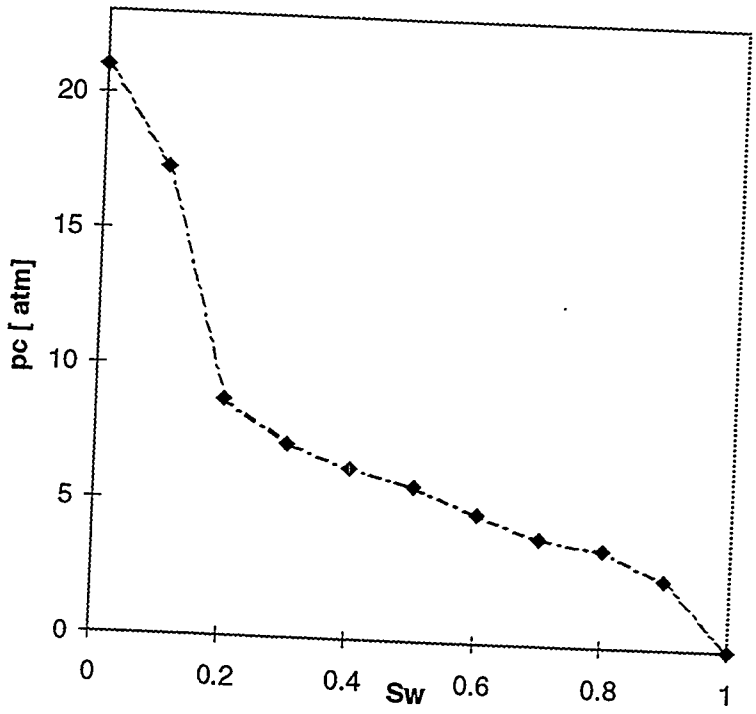

Fig. 3.7 Capillary pressure curve

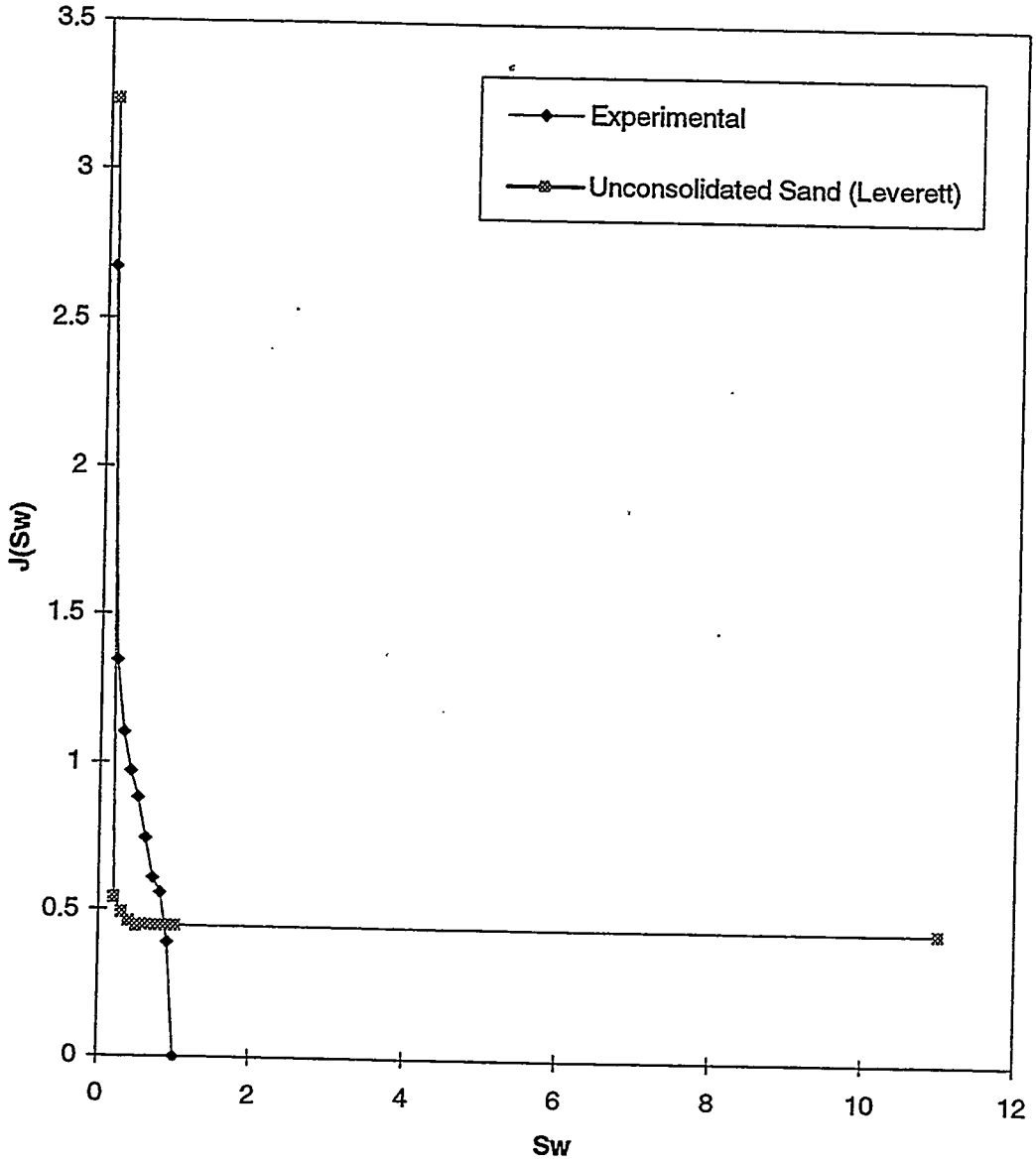

Fig. 3.8 Experimental Leverett Function

The results of the simulation for history matching of the saturation profile are shown in Fig. 3.9. The solid symbols represent the simulation results. A good match of the position and the shape of the front was obtained. The slope of the weight gain versus the square root of time obtained in this case was $0.4537 \pm 0.001 g / s^{1/2}$, which compared well with the experimental slope of $0.4331 g / s^{1/2}$ and represents an error of 4.7 %.

Because in this model we simultaneously match weight gain and saturation profiles for different times, our matches for the capillary pressure and water relative permeability curve are highly constrained.

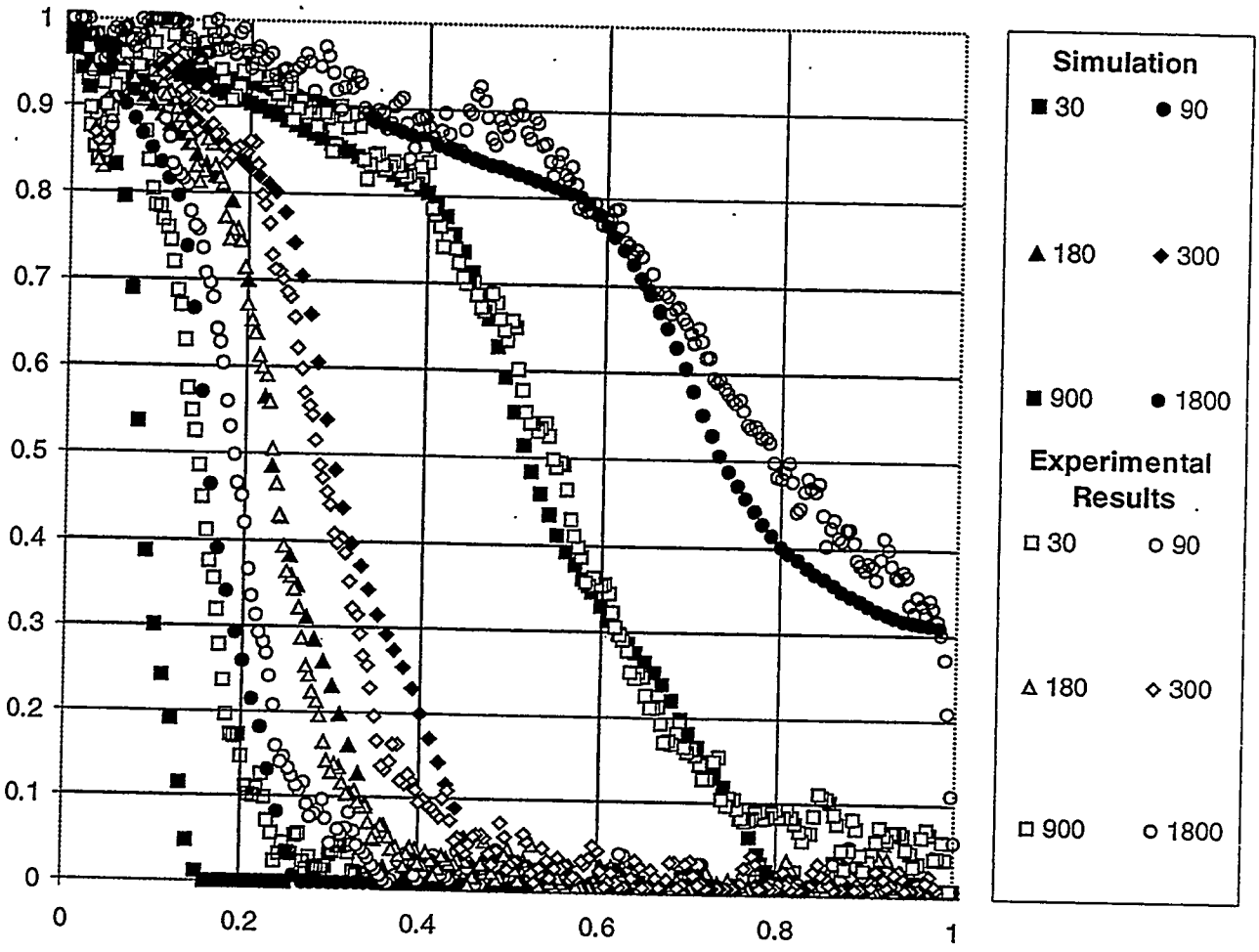

Fig. 3.9 Normalized saturation profile obtained by the method of non-linear regression

NOMENCLATURE

A	Relative permeability coefficient
A_c	Cross-sectional area
B	Exponent in power-law model for relative permeability curve
CT_{wet}	CT value for a fully water saturated core
CT_{dry}	CT value for the dry core
CT_{water}	CT value of water
CT_{air}	CT value of air
CT_{obj}	CT value of the image being processed
IP	Imbibition potential
$J(S_w)$	Leverett's J-function, dimensionless
k	Permeability
k_w	Effective water permeability
k_{rw}	Relative permeability of water
m	Mass of water imbibed
m_{wD}	Dimensionless volume imbibed
m_{wT}	Ultimate volume imbibed
P_c	Capillary pressure

P_{co}	Capillary pressure fitting parameter
Q_w	Volume of water imbibed
S_w	Water saturation
t	Time
t'	Dimensionless time
u_w	Darcy velocity of water
x	Position of the front

Greek and Symbols

ε	Y-intercept found by the linear fit of position of water saturation versus the square root of time
λ	Slope of linear fit of position of water saturation *versus* the square root of time
λ_{imb}	Slope of measured weight gain *versus* square root of time
ϕ	Porosity
ρ_w	Water density
μ_w	Water viscosity.
σ	Interfacial tension
τ	Square root of time; or $\sqrt{t}$

Subscripts

d	diatomite
s	sandstone

REFERENCES

1. Anderson, W.G : "Wettability Literature Survey- Part 5: The Effects of Wettability on Relative Permeability", Journal of Petroleum Engineering (Nov 1987) 1453 - 1468.

2. Babadagli, T. and Ershaghi, I.: "Imbibition Assisted Two-Phase Flow in Natural Fractures," SPE 24044, paper presented at the Western Regional Meeting of the Society of Petroleum Engineers, Bakersfield, (March 30-April 1, 1992).

3. Baticky, J.P., McCaffery, F.G., Hodgins, P.K., and Fisher, D.B.: "Interpreting Relative Permeability and Wettability From Unsteady-State Displacement Measurements" paper SPE 9403 presented at the SPE 55th Annual Technical Conference and Exhibition , Dallas, Sept 21-24, 1980.

4. Bear, Jacob: Dynamics of Fuids in Porous Media, Dover Publications, Inc. New York, 1988. pp 446-448.

5. Bentsen, R.G.: "Conditions Under which the Capillary Term May be Neglected," *J.Cdn.Pet.Tech. 17* (Oct-Dec. 1978), No. 4, 25-30.

6. Bhat,S.K., Castanier,L.M. and Kovscek, A.R.: "Unpublished results: Scanning Electron Microscopy and Mercury Porosimetry of Diatomite," (1997).

7. Blunt, M.J. and H.Scher: "Pore-Level Modeling of Wetting," Physical Review E: Statistical Physics, Plasmas, Fluids and Related Interdisciplinary Topics, *52* (6) (1995) 6837-6403.

8. Craig, F.F.: The reservoir Engineering Aspects of Waterflooding, Monograph Series, SPE Richardson, (1971) 3.

9. Cruz Hernandez, J. and Perez,C. : "Imbibition as a Dispersion Process," SPE 23748, paper presented in Second Latin American Petroleum Engineering Conference, II LAPEC, of the Society of Petroleum Engineers, Caracas, Venezuela (March 8-11, 1992).

10. Garg, A, Kovscek, A.R., Nikrakvesh, M., Castanier, L.M., and Patzek, T.W.: " CT Scan and Neural Network Technology for construction of Detailed Distribution of Residual Oil Saturation During Waterflooding," SPE 35737, paper presented at the Western Regional Meeting, Anchorage (May 22-24, 1996).

11. Garg, A., Zwahlen, E. and Patzek, T.W.: "Experimental and Numerical Studies of One-Dimensional Imbibition in Berea Sandstone," Proceedings of the Sixteenth Annual American Geophysical Union Hydrology Days, Fort Collins, CO (April 15-18, 1996).

12. Handy, L.L.: " Determination of Effective Capillary Pressure for Porous Media from Imbibition Data," Petroleum Transactions, AIME, 219 (1960) 75-80.

13. Kerig, P.D and Watson, A.T.: "A New Algorithm for estimating Relative Permeabilities from Displacement Experiments," *SPE Reservoir Engineering* (Feb 1987) 103-112.

14. Ilderton, D.C., Patzek T.W., Rector, and H.J. Vinegar, H.J.: "Passive Imaging of Hydrofractures in the South Belridge Diatomite," *SPE Formation Evaluation*, (March 1996) 46-54.

15. Kirkham, Don and Feng, C.L.: *Soil Sci.* (1949) 67,29.

16. Lai, W. and Brandt, H.: "A Pressure-History Matching Method for Determination of Relative Permeabilities," *SPE Reservoir Engineering* (May 1988) 651-661.

17. Leverett, M.C.: "Capillary Behavior in Porous Solids," Trans. AIME, *142* (1941) 152-169.

18. Mattax, C.C. and Kyte, J.R.: "Imbibition Oil Recovery from Fractured, Water Drive Reservoirs," SPEJ (June 1962), 177-84.

19. Saidi, A. M.: "Simulation of Naturally Fractured Reservoirs," SPE 12270 presented at the 1983 Symposium on Reservoir Simulation, San Francisco (Nov.16-18, 1983).

20. Schwartz, D.E.: "Characterizing the Lithology, Petrophysical Properties, and Depositional Setting of the Belridge Diatomite, South Belridge Field, Kern County, California,"Studies of Geology of San Joaquin Basin, S. A. Graham and H. C. Olson, (Eds.), Society of Economic Paleontologists and Mineralogists, Los Angeles, (1988) 281-302.

21. "Shell Expanding Belridge Diatomite Program," *Oil and Gas Journal, 92* (April 11, 1994) 40-42.

22. Sigmund, P.M. and McCaffery, F.G.: "An Improved Unsteady-State Procedure for Determining the Relative Permeability Characteristics of Heterogeneous Porous Media," *SPEJ* (Feb. 1979) 15-28.

15. Stosur, J.J. and A. David: "Petrophysical Evaluation of the Diatomite Formation of the Lost Hills Field, California," *Journal of Petroleum Tech., 28* (October,1971) 1138-1144.

16. Watson, A.T., Richmond, P.C., Kerig, P.D, and Tao, T.M.: "A Regression-Based Method for Estimating Relative Permeabilities From Displacement Experiments," SPE Reservoir Engineering (Aug 1988) 953-958.

16. Zhang, X., Morrow, N., and Ma, S.: "Experimental Verification of a Modified Scaling Group for Spontaneous Imbibition," SPE 30762, paper presented at the SPE Annual Technical Conference and Exhibition, Dallas (Oct 22-25, 1995).

Appendix A
Source Code used for
Linear Regression Analysis

```
/*
*************************************************************************
```
File : ***labreg.cpp - Main File***

This program applies linear regression to examine the correlation between an independent variable, x, and a dependent variable, y. The program uses the class LinRegANOVA and
Linreg defined in file *linreg.hpp* and implemented in file *linreg.cpp*

File from example TSLINREG.CPP test program in
Shammas, N.C., "C/C++ Mathematical Algorithms for Scientists and Engineers," Mc.Graw-Hill, Inc. New York, 1995.

Modified by :
Josephina Schembre
Stanford University, Oct. 24th 1997

```
*************************************************************
*/

// ---------------------------
#include <stdlib.h>
#include <string.h>
#include <fstream.h>
#include <iostream.h>
#include <time.h>
#include <stdio.h>
#include <math.h>
#include "linreg.hpp"
#include "global.h"
// ---------------------------

#define MAX_FX 4
int LINES=5000;
int START=10;

//-------------------------
// FUNCTION PRESSANYKEY()
//-------------------------
void pressAnyKey()
{
        printf("\n Press any key to continue...");
        getchar();
        puts("\n\n");
}
```

```
//-----------------------
// FUNCTION fx()
//-----------------------

double fx(double x)
{
        return x;
}

//-----------------------
// FUNCTION fy()
//-----------------------
double fy(double x)
{
        return x;
}

//---------------------
// FUNCTION ify()
//---------------------

double ify(double x)
{
        return x;
}

//---------------------
// FUNCTION LINEAR()
//---------------------

double linear(double x)
{
        return x;
}

//---------------------
// FUNCTION lN()
//---------------------

double ln(double x)
{
        return log(x);
}
//-----------------------------------
```

```
// FUNCTION READMATRIX()
//--------------------------------------

void ReadMatrix(Matrix mat, int size)
{
        double time;
        int col=0;


        ifstream infile;
        infile.open("diatom1.txt",ios::in);

        if (!infile)
        {
        cout << "error opening file" << endl;
        exit(0);
        }

        cout << "infile opened" << endl;


        for (int j=0; j<=(START-1);j++)
        {
        infile.ignore(80,'\n');
        }

        for (int i=0; i<=(size-1); i++)
        {
                infile >> time >> mat(i,col) >> mat(i,col+1);
                infile.ignore(20,'\n');
        }
        infile.close();
}

// ---------------------------
//  Main Function
// ---------------------------
main()
{
        int SIZE;
        SIZE= LINES - START;
        Matrix mat(SIZE,5);
        LinReg r;
        double (*fxArr[MAX_FX])(double);
```

```
        double (*fyArr[MAX_FX])(double);
        double probability;
        double slopeHi, slopeLow;
        double intHi, intLow;
        double testValue, calcT, tableT;
        BestLinReg bestR2[MAX_FX];
        int numFx= MAX_FX;
        int i;
        int passTest;

        ReadMatrix(mat,SIZE);


r.Initialize(fx,fy,ify,0,1,FALSE,0);
r.sumLinReg(mat,SIZE);
r.DoLinReg();

printf("******************** Linear Regression***************\n");
printf("Number of Points:%lg\n", r.getSum());
printf("R^2=%lg\n", r.getSlope());
printf("Intercept=%lg\n",r.getIntercept());

pressAnyKey();

printf("********************** ANOVA *************************\n");
printf("Regression SS = %lg\n", r.ANOVA.Reg_SS);
printf("Regression df=%lg\n", r.ANOVA.Reg_df);
printf("Residual SS = %lg\n", r.ANOVA.Residual_SS );
printf("Residual df = %lg\n" , r.ANOVA.Residual_df);
printf("Total SS = %lg\n", r.ANOVA.Total_SS);
printf("Total df = %lg\n", r.ANOVA.Total_df);

printf("S^2=%lg\n", r.ANOVA.S2);
printf("F=%lg\n",r.ANOVA.LINREG_F);

printf("*************************************************************\n");

pressAnyKey();

}
```

```
#ifndef _LINREG_HPP_
#define _LINREG_HPP_

/*
*************************************************************************
 File : linreg.hpp - Declaration file

   Copyright (c) 1995 Namir C. Shammas

   Version 1.0                  Date 6/18/94

   C++ module which performs the following linear regression operations:

      + Basic linear regression
      + Confidence interval for regression coefficients
      + Testing regression coefficients
      + Automatic best linearized fit

   Modified by:

         Josephina Schembre
         Stanford University
         October 24th, 1997

*************************************************************************
*/

#include "arrays.hpp"

#define LINREG_MAX_FUNCTIONS 64

/* ANOVA table record structure */

class LinRegANOVA {
 public:
  double Reg_df;
  double Reg_SS;
  double Residual_df;
  double Residual_SS;
  double Total_df;
  double Total_SS;
  double S2;
  double LINREG_F;};
/* Linear regression record structure */
```

```
class LinReg {

public:
 LinReg() {}

 void Initialize(double (*Fx)(double),
       double (*Fy)(double),
       double (*InvFy)(double),
       int XIndex, int YIndex,
       int HasMissingData,
       double MissingCode);

 double getSlope()
   { return Slope; }
 double getIntercept()
   { return Intercept; }
 double getR2()
   { return R2; }
 double getSum()
   { return sum; }

 void sumLinReg(Matrix& DataMat, int NData);

 void DoLinReg();

 void YhatCI(double xr, double probability,
        double& yHat, double& yHi, double& yLow);

 void LinRegCoefCI(double probability,
             double& slopeHi, double& slopeLow,
             double& intHi, double& intLow);

 void LR_Slope_T_test(double probability, double testValue,
              double& calcT, double& tableT,
              int& passTest);

 void LR_Int_T_test(double probability, double testValue,
             double& calcT, double& tableT,
             int& passTest);

 void LR_R2_T_Test(double probability,
            double& calcT, double& tableT, int& passTest);
 LinRegANOVA ANOVA;
```

```
 protected:
  int Xindex;
  int Yindex;
  int hasMissingData;
  double (*fx)(double);
  double (*fy)(double);
  double (*Invfy)(double);
  double missingCode;
  double sumX;
  double sumXX;
  double sum;
  double sumY;
  double sumYY;
  double sumXY;
  /* basic statsitics */
  double MeanX;
  double MeanY;
  double SdevX;
  double SdevY;
  double Slope;
  double Intercept;
  double R2;
  /* Regression results */
  double StdErSlope;
  double StdErIntercept;};

class BestLinReg {
 public:
  int fxIndex;
  double R2;
  double Slope;
  double Intercept;};

int BestFit(Matrix& DataMat,
        int NData, int numTrnsFx,
        int Xindex, int Yindex,
        double (*fx[LINREG_MAX_FUNCTIONS])(double),
        double (*fy[LINREG_MAX_FUNCTIONS])(double),
        BestLinReg* r);

#endif
```

```
/*
*************************************************************************
```

File : ***linreg.cpp -Implementation file***

Copyright (c) 1995 Namir C. Shammas

Version 1.0 Date 6/18/94

C++ module which performs the following linear regression operations:

+ Basic linear regression
+ Confidence interval for regression coefficients
+ Testing regression coefficients
+ Automatic best linearized fit

Modified by:

Josephina Schembre
Stanford University
October 24th, 1997

```
*************************************************************************
*/

#include <stdlib.h>
#include <math.h>
#include "global.h"
#include "linreg.hpp"
#include "statlib.h"

void LinReg::Initialize(double (*Fx)(double),
                        double (*Fy)(double),
                        double (*InvFy)(double),
                        int XIndex, int YIndex,
                        int HasMissingData,
                        double MissingCode)
/* initialize statistical summations and data range */
{
 sumX = 0;
 sumXX = 0;
 sum = 0;
 sumY = 0;
 sumYY = 0;
 sumXY = 0;
```

```
  hasMissingData = HasMissingData;
  missingCode = MissingCode;
  fx = Fx;
  fy = Fy;
  Invfy = InvFy;
  Xindex = XIndex;
  Yindex = YIndex;
}

void LinReg::sumLinReg(Matrix& DataMat, int NData)
/* update statistical summations */
{
  int i;
  double xr, yr;
  double (*ffx)(double);
  double (*ffy)(double);

  ffx = fx;
  ffy = fy;

  for (i = 0; i < NData; i++) {
    xr = DataMat(i, Xindex);
    yr = DataMat(i, Yindex);
    if (!(hasMissingData &&
        ((xr <= missingCode) ||
        (yr <= missingCode)))) {
      /* transform x and y data */
      xr = (*ffx)(xr);
      yr = (*ffy)(yr);
      /* Update summations */
      sum += 1;
      sumXY += xr * yr;
      sumX += xr;
      sumXX += SQR(xr);
      sumY += yr;
      sumYY += SQR(yr);
    }
  }
}



void LinReg::DoLinReg()
/* calculate regression coefficients and related results */
```

```
{
 double S;
 MeanX = sumX / sum;
 MeanY = sumY / sum;
 SdevX = sqrt((sumXX - SQR(sumX) / sum) /
              (sum - 1));
 SdevY = sqrt((sumYY - SQR(sumY) / sum) /
              (sum - 1));
 Slope = (sumXY - MeanX * MeanY * sum) /
          SQR(SdevX) / (sum - 1);
 Intercept = MeanY - Slope * MeanX;
 R2 = SQR(Slope * SdevX / SdevY);
 ANOVA.Reg_SS = SQR(sumXY - sumY * MeanX) /
                (SQR(SdevX) * (sum - 1));
 ANOVA.Total_SS = sumYY - SQR(sumY) / sum;
 ANOVA.Residual_SS = ANOVA.Total_SS - ANOVA.Reg_SS;
 ANOVA.Residual_df = sum - 2;
 S = sqrt(ANOVA.Residual_SS / ANOVA.Residual_df);
 StdErSlope = S / sqrt(sumXX - SQR(sumX) / sum);
 StdErIntercept = S * sqrt(sumXX / sum /
                  SQR(SdevX) / (sum - 1));
 ANOVA.Reg_df = 1;
 ANOVA.Total_df = sum - 1;
 ANOVA.S2 = S * S;
 ANOVA.LINREG_F = ANOVA.Reg_SS / ANOVA.S2;
}

void LinReg::YhatCI(double xr, double probability,
          double& yHat, double& yHi, double& yLow)
/* calculate projections and their confidence interval */
{
 double Df, deltaY, p, tableT;
 double (*ffx)(double);
 double (*iffy)(double);

 ffx = fx;
 iffy = Invfy;

 if (probability > 1 )
   p = 0.5 - probability / 200;
 else
   p = 0.5 - probability / 2;
 Df = sum - 2;
 tableT = TInv(p, Df);
```

```
  xr = (*ffx)(xr); /* transform xr */
  deltaY = sqrt(SQR(xr - MeanX) /
          (SQR(sumX) * (sum - 1))+1/
          (sum+1)) * sqrt(ANOVA.S2) * tableT;
  yHat = Intercept + Slope * xr;
  yHi= (*iffy)(yHat + deltaY);
  yLow = (*iffy)(yHat - deltaY);
  yHat = (*iffy)(yHat);
}

void LinReg::LinRegCoefCI(double probability,
                  double& slopeHi, double& slopeLow,
                  double& intHi, double& intLow)
/* calculate confidence interval for slope and intercept */
{
 double Df, tableT, diff, p;

 if (probability > 1)
   p = 0.5 - probability / 200;
 else
   p = 0.5 - probability / 2;
 Df = sum - 2;
 tableT = TInv(p, Df);
 diff = tableT * StdErSlope;
 slopeHi = Slope + diff;
 slopeLow = Slope - diff;

 diff = tableT * StdErIntercept;
 intHi = Intercept + diff;
 intLow = Intercept - diff;
}

void LinReg::LR_Slope_T_test(double probability,
                  double testValue,
                  double& calcT, double& tableT,
                  int& passTest)
/* compare slope value with a tested value
   Hypothesis tested is H0: Slope = testValue  */
{
 double Df, p;

 if (probability > 1)
   p = 0.5 - probability / 200;
 else
```

```
    p = 0.5 - probability / 2;
  Df = sum - 2;
  tableT = TInv(p, Df);
  calcT = (Slope - testValue) / StdErSlope;
  passTest = (fabs(calcT) <= tableT) ? TRUE : FALSE;
}

void LinReg::LR_Int_T_test(double probability,
                    double testValue,
                    double& calcT, double& tableT,
                    int& passTest)
/* compare intercept value with a tested value
   Hypothesis tested is H0: Intercept = testValue */
{
  double Df, p;

  if (probability > 1)
    p = 0.5 - probability / 200;
  else
    p = 0.5 - probability / 2;
  Df = sum - 2;
  tableT = TInv(Df,p);
  calcT = (Intercept - testValue) / StdErIntercept;
  passTest = (fabs(calcT) <= tableT ) ? TRUE : FALSE;
}

void LinReg::LR_R2_T_Test(double probability,
                    double& calcT, double& tableT,
                    int& passTest)
/* Procedure to test hypothesis H0 : R^2 = 0 */
{
  double p, Df;

  if (probability > 1)
    p = 0.5 - probability / 200;
  else
    p = 0.5 - probability / 2;
  Df = sum - 2;
  tableT = TInv(p, Df);
  calcT = sqrt(R2 * Df / (1 - R2));
  passTest = (calcT <= tableT) ? TRUE : FALSE;
}

int BestFit(Matrix& DataMat,
```

```
        int NData, int numTrnsFx,
        int Xindex, int Yindex,
        double (*fx[LINREG_MAX_FUNCTIONS])(double),
        double (*fy[LINREG_MAX_FUNCTIONS])(double),
        BestLinReg* r)
/* find the best model to fit the data */
{
 double sum, sumX, sumXX, sumY, sumYY, sumXY;
 double MeanX, MeanY, SdevX, SdevY;
 double x, y;
 int i, j, offset, inOrder;
 BestLinReg temp;

 if (Xindex == Yindex ||
     NData < 3 ||
     numTrnsFx < 2)
   return FALSE;

 /* iterate over the functions */
 for (i = 0; i < numTrnsFx; i++) {
   /* initialize summations */
   sum = 0;
   sumX = 0;
   sumXX = 0;
   sumY = 0;
   sumYY = 0;
   sumXY = 0;
   /* process the observations */
   for (j = 0; j < NData; j++) {
     x = (*fx[i])(DataMat(j, Xindex));
     y = (*fy[i])(DataMat(j, Yindex));
     sum++;
     sumX += x;
     sumY += y;
     sumXX += SQR(x);
     sumYY += SQR(y);
     sumXY += x * y;
   }
   /* calculate the results */
   MeanX = sumX / sum;
   MeanY = sumY / sum;
   SdevX = sqrt((sumXX - SQR(sumX) / sum) /
                (sum - 1));
   SdevY = sqrt((sumYY - SQR(sumY) / sum) /
```

```
                (sum - 1));
    (r+i)->Slope = (sumXY - MeanX * MeanY * sum) /
            SQR(SdevX) / (sum - 1);
    (r+i)->Intercept = MeanY - (r+i)->Slope * MeanX;
    (r+i)->R2 = SQR((r+i)->Slope * SdevX / SdevY);
    (r+i)->fxIndex = i;
  }
  /* sort the results in descending order */
  offset = numTrnsFx;
  do {
    offset = (offset * 8) / 11;
    offset = (offset == 0) ? 1 : offset;
    inOrder = TRUE;
    for (i = 0; i < (numTrnsFx - offset); i++) {
      j = i + offset;
      /* swap elements? */
      if ((r+i)->R2 < (r+j)->R2) {
        inOrder = FALSE;
        temp = *(r + i);
        *(r + i) = *(r + j);
        *(r + j) = temp;
      }
    }
  } while (!(offset == 1 && inOrder == TRUE));
  return TRUE;
}
```

Appendix B
Data Input File used for Numerical Simulation in ECLIPSE®

--

-- **ECLIPSE INPUT FILE - *LAB.DATA***

-- IMBIBITION PERFORMANCE OF A L= 8.43 cm, D=2.5 cm Cylindrical core.

-- Water-air imbibition Diatomite , Permeability = 8.0 mD .

-- Porosity = 65 %

RUNSPEC

= NDIVIX NDIVIY NDIVIZ QRDIAL NUMRES QNNCON MXNAQN MXNAQC

QDPORO QDPERM

1 1 102 T 1 F 0 0 F F/

= OIL WATER GAS DISGAS VAPOIL

F T T F F F /

= UNIT CONVENTION

'LAB' /

= NRPVT NPPVT NTPVT

1 13 1 1 F T /

= NSSFUN NTSFUN QDIRKR QREVKR

50 2 F T F F /

= NDRXVD NTEQUL NDPRVD

20 1 100 F F T F 1 /

= NTFIP

8 F F /

= NWMAXZ NCWMAX NGMAXZ NWGMAX

2 1 4 2 /

= QIMCOL NWCOLC NUPCOL

F 0 4 /

= MXMFLO MXMTHP MXMWFR MXMGFR MXMALQ NMMVFT

0 0 0 0 0 0 /

= MXSFLO MXSTHP NMSVFT

0 0 0 /

= NAQFET NCAMAX

0 0 /

= DAY MONTH YEAR

1 'JAN' 1998 /

= QSOLVE NSTACK QFMTOU QFMTIN QUNOUT QUNINP NGDISK IDYNAM

QOPT9P

T 30 T F T F/

GRID

==========

DRV

1.250 /

DTHETAV

360. /

```
DZ
  1*54.8
  100*0.0843
  1*54.8 /

INRAD
0.0001/
---
BOX
--- IX1-IX2  JY1-JY2       KZ1-KZ2
       1 1    1 1    1 1    /
PERMR
   1*1000 /
PERMTHT
   1*1000 /
PERMZ
   1*1000 /
PORO
   1*1000 /
```

```
---
BOX
--- IX1-IX2  JY1-JY2  KZ1-KZ2
   1  1    1  1    2  101   /
PERMR
  100*8.0 /
PERMTHT
  100*8.0 /
PERMZ
  100*8.0 /
PORO
   100*0.65 /
BOX
--- IX1-IX2  JY1-JY2  KZ1-KZ2
   1  1    1  1    102 102  /
PERMR
       1*17000. /
PERMTHT
       1*17000. /
PERMZ
       1*17000. /
```

```
PORO
      1*1000. /
--- TOP Specification
BOX
--- IX1-IX2  JY1-JY2 KZ1-KZ1
      1 1   1 1   1 1/
TOPS
   1 /
RPTGRID
0 0 0 0 0 1 0 0 0 1 0 0 1 /

PROPS  ==========================================
DENSITY
   1.0    1.0    1.0  /
PVDG
-- PRESSURE  FVF       VISC
       1.0       1.00      1.812E-2
      1.05    09.523E-1    1.814E-2 /
PVTW
--      PREF   Bw    Cw    Visc   Viscdp
           1.  1.00   5E-05  1.0     0.0 /
```

ROCK

3.0 0.5E-08 /

SWFN

-- Sw Krw Pcw

0.0 0.0 21

0.1 0.003028 17.3282

0.2 0.00303 8.72709

0.3 0.043461 7.169071

0.4 0.058 6.307392

0.5 0.059505 5.734277

0.6 0.069285 4.817148

0.7 0.137761 3.944111

0.8 0.18 3.623157

0.9 0.19 2.52932

1.0 0.22 0.000 /

-- Sw Krw Pcw

0.0 0.0 0.0

1.0 1.0 0.0 /

```
SGFN
--  Sg    Krg     Pcg
    0.0   0.0     0.0
    0.1   0.01    0.0
    0.2   0.04    0.0
    0.3   0.09    0.0
    0.4   0.16    0.0
    0.5   0.25    0.0
    0.6   0.36    0.0
    0.7   0.49    0.0
    0.8   0.64    0.0
    0.9   0.81    0.0
    1.0   1.0     0.0 /
/

RPTPROPS
    2*1 0  2*1 0 2*1   /
```

```
REGIONS    ====================================

BOX

-- IX1-IX5  JY1-JY1  KZ1-KZ14

   1  1    1  1  1  1 /

SATNUM

   1*2 /

FIPNUM

   1*2 /

BOX

-- IX1-IX5  JY1-JY1  KZ1-KZ14

   1   1     1     1     2     101 /

SATNUM

   100*1 /

FIPNUM

   100*2 /

BOX

--- IX1-IX5  JY1-JY1  KZ1-KZ14

   1      1   1     1     102   102 /

SATNUM

   1*2 /
```

```
FIPNUM
   1*3 /
RPTREGS
   0 1 0 1 /

SOLUTION ==========

SWAT
   1*0.0
   100*0.0
   1*1.0      /

PRESSURE
--       Pressure
        101*1
          1*1.0265 /
RPTSOL
   1 0 1 1 0 0 2  7*0 0 0 0 0  /
```

SUMMARY ==========

RUNSUM

RWIP

1 2 3 /

BWSAT

1 1 101 /

1 1 100 /

1 1 99 /

1 1 98 /

1 1 97/

1 1 96 /

1 1 95 /

1 1 94 /

1 1 93 /

1 1 92 /

1 1 91 /

1 1 90 /

1 1 89 /

1 1 88 /

1 1 87 /

1 1 86 /

1 1 85 /

1 1 84 /

1 1 83 /

1 1 82 /

1 1 81 /

1 1 80 /

1 1 79 /

1 1 78 /

1 1 77 /

1 1 76 /

1 1 75 /

1 1 74 /

1 1 73 /

1 1 72 /

1 1 71 /

1 1 70 /

1 1 69 /

1 1 68 /

1 1 67 /

1 1 66 /

1 1 65 /

1 1 64 /

1 1 63 /

1 1 62 /

1 1 61 /

1 1 60 /

1 1 59 /

1 1 58 /

1 1 57 /

1 1 56 /

1 1 55 /

1 1 54 /

1 1 53 /

1 1 52 /

1 1 51 /

1 1 50 /

1 1 49 /

1 1 48 /

1 1 47 /

1 1 46 /

1 1 45 /

1 1 44 /

1 1 43 /

1 1 42 /

1 1 41 /

1 1 40 /

1 1 39 /

1 1 38 /

1 1 37 /

1 1 36 /

1 1 35 /

1 1 34 /

1 1 33 /

1 1 32 /

1 1 31 /

1 1 30 /

1 1 29 /

1 1 28 /

1 1 27 /

1 1 26 /

1 1 25 /

1 1 24 /

1 1 23 /

1 1 22 /

1 1 21 /

1 1 20 /

1 1 19 /

1 1 18 /

1 1 17 /

1 1 16 /

1 1 15 /

1 1 14 /

1 1 13 /

1 1 12 /

1 1 11 /

1 1 10 /

1 1 9 /

1 1 8 /

1 1 7 /

1 1 6 /

1 1 5 /

1 1 4 /

1 1 3 /

1 1 2 /

/

```
-- SUMMARY REPORT


RPTSMRY

1 /

--Turn on run summary at end of PRT file.

RUNSUM


SCHEDULE ==========

RPTSCHED

      /

TUNING

 .000277 0.001  0.0000277 /

 /

  /


 TSTEP

    45*0.067 /

 END
```